4942.4-E

AN EXPERIMENTAL INVESTIGATION OF THE EFFECT OF ELECTRICALLY INDUCED CONTROLLED FREQUENCY PERTURBATIONS ON BOUNDARY LAYER TRANSITION

Jeffrey J. Ketcham
Henry R. Velkoff

Technical Report

Contract No. DA-31-124-ARO-D-246

U. S. Army Research Office - Durham
Box CM, Duke Station
Durham, North Carolina 27706

June, 1967

The Ohio State University Research Foundation
Columbus, Ohio 43212

DISCLAIMER

The findings in this report are not to be construed as an official Department of the Army position unless so designated by other authorized documents.

****

The citation of trade names and names of manufacturers in this report is not to be construed as official Government endorsement of approval of commercial products or services references.

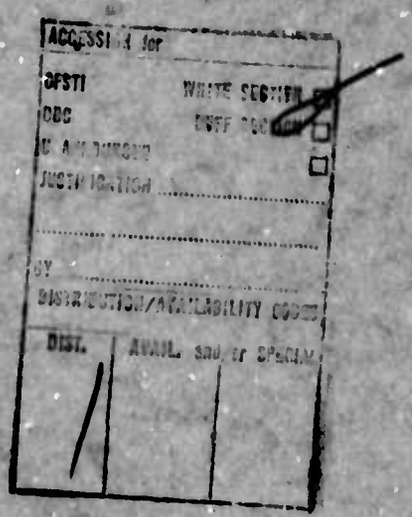

RF Project 1864

Report No. 5

TECHNICAL

REPORT

By

THE OHIO STATE UNIVERSITY
RESEARCH FOUNDATION

1314 KINNEAR RD.
COLUMBUS, OHIO 43212

To U. S. ARMY RESEARCH OFFICE - DURHAM
Box CM, Duke Station
Durham, North Carolina 27706
Contract No. DA-31-124-ARO-D-246
Project Nos. 2001050B700, 1D121404142

On AN EXPERIMENTAL INVESTIGATION OF THE EFFECT OF ELECTRICALLY INDUCED CONTROLLED FREQUENCY PERTURBATIONS ON BOUNDARY LAYER TRANSITION

Submitted by Jeffrey J. Ketcham and Henry R. Velkoff
Department of Mechanical Engineering

Date June, 1967

FOREWORD

This report presents essentially the same material as the Master's Thesis, "An Experimental Investigation of the Effect of Electrically Induced Controlled Frequency Perturbations on Boundary-Layer Transition," by Jeffrey Ketcham. The thesis was presented in partial fulfillment of the requirements for the Master of Science in Mechanical Engineering at The Ohio State University.

Specific thanks are given to the support given to this study by both the Battelle Memorial Institute through the use of some of their equipment and facilities as well as the U. S. Army Research Office - Durham. At Battelle Institute specific thanks are given to J. E. Gates, W. E. Kortear, R. Badertscher, V. O. Hoehne, and D. Aithen, for their assistance in bringing this project to fruition. The junior author also wishes to express his thanks to Dr. Henry R. Velkoff for his suggestion of topic, persistent encouragement and help in the conduct of this research.

ABSTRACT

An experimental investigation was conducted to determine the effects of corona discharge on boundary-layer transition. A flat plate was mounted in Battelle Memorial Institute's low-turbulence wind tunnel. The location of transition was determined using a near-surface impact pressure probe. Boundary-layer excitation was accomplished by suspending a series of corona wires parallel to the plate outside the boundary layer. It was found that, under certain conditions, the transition point could be moved downstream upon application of a steady potential to the wires. Superposition of a pulsating potential did not influence the results over a wide range of pulsation frequency.

TABLE OF CONTENTS

	Page
LIST OF TABLES	v
LIST OF ILLUSTRATIONS	vi
NOMENCLATURE	ix
INTRODUCTION	1
THEORY OF BOUNDARY-LAYER OSCILLATIONS	3
ELECTRICAL PERTURBATIONS	13
EXPERIMENTAL INVESTIGATION	17
DESIGN OF THE EXPERIMENT	17
EXPERIMENTAL APPARATUS	19
EXPERIMENTAL PROCEDURE	27
EXPERIMENTAL CALCULATIONS	28
RESULTS OF EXPERIMENTAL INVESTIGATION	32
OBTAINING A LAMINAR BOUNDARY LAYER	32
DETECTING TRANSITION	34
THE EFFECT OF ELECTRICAL PERTURBATIONS ON TRANSITION	39
DISCUSSION OF RESULTS	46
SUMMARY OF CONCLUSIONS AND RECOMMENDATIONS	50
ILLUSTRATIONS	53
LIST OF REFERENCES	91

LIST OF TABLES

Table		Page
1.	FACTORS INFLUENCING TRANSITION.	2
2.	NEUTRAL-STABILITY CURVE	9
3.	CORONA VARIABLES.	16
4.	VELOCITY RATIOS FOR A LAMINAR BOUNDARY LAYER ALONG A FLAT PLATE.	37
5.	TRANSITION CONFIRMATION, 164 FPS FEET PER SECOND.	38

LIST OF ILLUSTRATIONS

Figure		Page
1.	NEUTRAL STABILITY CURVE IN TERMS OF REYNOLDS NUMBER AND FREQUENCY PARAMETER	53
2.	NEUTRAL STABILITY CURVE IN TERMS OF REYNOLDS NUMBER AND WAVELENGTH PARAMETER	54
3.	NEUTRAL STABILITY CURVE IN TERMS OF REYNOLDS NUMBER AND VELOCITY PARAMETER	55
4.	NEUTRAL STABILITY CURVE IN TERMS OF REYNOLDS NUMBER (Re_x) AND FREQUENCY	56
5.	NEUTRAL STABILITY CURVE IN TERMS OF REYNOLDS NUMBER (Re_x) AND WAVELENGTH	57
6.	NEUTRAL STABILITY CURVE IN TERMS OF REYNOLDS NUMBER (Re_x) AND VELOCITY PARAMETER	58
7.	SECTION VIEW OF FLAT PLATE LEADING EDGES	59
8.	FLAT PLATE STATIC PRESSURE TAPS	60
9.	REARWARD VIEW OF ACTIVE SIDE OF PLATE	61
10.	DOWNSTREAM VIEW OF TEST SECTION	62
11.	FLAT PLATE MOUNTING DETAIL	63
12.	ELEVATION VIEW OF WIND TUNNEL	64
13.	WIND TUNNEL EXHAUST FAN AND MOTOR	65
14.	HORIZONTAL DISTRIBUTION OF DYNAMIC PRESSURE AT CENTERLINE OF TEST SECTION	66
15.	WALL BOUNDARY LAYER AT THE VERTICAL CENTERLINE OF WIND TUNNEL TEST SECTION	67
16.	WIND TUNNEL AIR INTAKE AREA	68
17.	TURBULENCE SCREENS NEAR WIND TUNNEL AIR INTAKE AREA	69
18.	IMPACT PRESSURE IN THE BOUNDARY LAYER AT A SMALL CONSTANT HEIGHT ABOVE THE SURFACE	70

LIST OF ILLUSTRATIONS (Continued)

Figure		Page
19.	CLOSEUP OF A GLASS PRESSURE PROBE TIP	71
20.	UNDERSIDE OF PLATE SHOWING PRESSURE PROBE ASSEMBLY AND CORONA WIRES.	72
21.	UPSTREAM VIEW OF ACTIVE SIDE OF PLATE	73
22.	PULSATING POTENTIAL IMPOSED ON CORONA WIRES	74
23.	CIRCUIT DIAGRAM	75
24.	ELECTRICAL EQUIPMENT AND TEST SECTION EXTERIOR.	76
25.	MANOMETER BOARD FOR INDICATING STATIC PRESSURE DISTRIBUTION OVER PLATE	77
26.	TYPICAL STATIC PRESSURE DISTRIBUTION OVER PLATE SURFACE	78
27.	TUNNEL CONTROL CONSOLE SHOWING BAROMETER AND FLOW CONTROL MANOMETERS.	79
28.	WIND TUNNEL FLOW ADJUSTMENT DOORS	80
29.	NEAR SURFACE IMPACT PRESSURE WITH ROUNDED LEADING EDGE.	81
30.	NEAR SURFACE IMPACT PRESSURE WITH SHARP LEADING EDGE. . .	82
31.	TYPICAL IMPACT PRESSURE PROFILES INDICATING BOUNDARY-LAYER TRANSITION	83
32.	TOP SIDE OF PLATE SHOWING STATIONARY IMPACT PRESSURE PROBE.	84
33.	FREQUENCY PARAMETER VERSUS REYNOLDS NUMBER FOR $\delta^* = 0.24$	85
34.	CONTROL TESTS, FLOW SPEED 175 FEET PER SECOND	86
35.	CORONA TEST, FLOW SPEED 175 FEET PER SECOND	87
36.	CORONA TEST, FLOW SPEED 153 FPS	88

LIST OF ILLUSTRATIONS (Continued)

Figure

Page

37. SHIFT OF TRANSITION BY CORONA DISCHARGE 89

38. IMPACT PRESSURE AS A FUNCTION OF THE FREQUENCY OF THE ELECTRICAL PERTURBATION 90

NOMENCLATURE

Symbol		Units
A	Amplitude of boundary-layer oscillation	ft
c_r	Velocity of boundary-layer oscillation	ft/sec
$\bar{E}$	Electric field strength	volts/ft
f	Frequency	cps
K	Ion mobility	ft^2/volt-sec
p	Total pressure	lb/ft^2
p'	Fluctuating component of pressure	lb/ft^2
P	Steady component of pressure	lb/ft^2
R	Gas constant	$ft\text{-}lb_f/lb_m\text{-}°R$
Re	Reynolds Number	dimensionless
t	Time	sec
u	Total velocity in x direction	ft/sec
u'	Fluctuating velocity in x direction	ft/sec
U	Steady velocity in x direction	ft/sec
U_m	Maximum velocity in x direction	ft/sec
v	Total velocity in y direction	ft/sec
v'	Fluctuating velocity in y direction	ft/sec
V	Steady velocity in y direction	ft/sec
$\bar{v}_t$	Total ion velocity	ft/sec
$\bar{v}_a$	Air velocity in corona wind	ft/sec
w	Total velocity in z direction	ft/sec
w'	Fluctuating velocity in z direction	ft/sec

NOMENCLATURE (Continued)

Symbol		Units
W	Steady velocity in z direction	ft/sec
x	Distance along plate	ft
y	Distance normal to plate	ft
z	Distance normal to x and y	ft
α	Reciprocal of oscillation wavelength	ft^{-1}
β_i	Amplification factor for oscillations	sec^{-1}
β_r	Circular frequency of oscillations	rad/sec
δ	Boundary-layer thickness	ft
δ^*	Momentum thickness	ft
η	Similarity parameter	dimensionless
λ	Oscillation wavelength	ft
μ	Viscosity	$lb_m/ft\text{-}sec$
ν	Dynamic viscosity	ft^2/sec
ρ	Density	lb_m/ft^3
ψ	Stream function	ft^2/sec

Subscripts

L	Laminar
T	Turbulent
tr	Transition

INTRODUCTION

Investigations of the transition of laminar-to-turbulent flow date back to the pipe and channel studies of O. Reynolds[1*] in 1883. Such work was prompted by the increased pressure gradient required to maintain flow in a turbulent regime. No less significant today are the effects of boundary-layer transition on the performance of airfoils, heat exchangers, and essentially all devices concerned with fluid motion, for associated with transition, are marked changes in surface friction drag and heat-transfer rate. While many investigations over the years have contributed to the characterization of turbulent flow, much is yet to be learned regarding the detailed physical mechanisms of transition and possible means for its control.

It is well known that the transition phenomenon is sensitive to a number of flow conditions. Some of these are given below in Table 1[2]. Additionally, it has been experimentally demonstrated that transition may be forestalled by employing a flexible surface skin, or initiated, by a tripping device or sonic excitation. Flexible skin for delaying transition and reducing surface drag was first proposed by Kramer as a result of studies on the hydrodynamic performance of dolphins. Kramer's experimental results[3] with flexible surface coatings in water showed that reduction of skin friction coefficients by a factor of two is possible under certain conditions. Prandtl first demonstrated the effect of a tripping wire in artificially inducing

---

* Superscripts denote items appearing in the List of References.

transition on a sphere in 1914. More recent investigations have illustrated the transitional effects of jet engine noise[4], loudspeakers in the flow[5], and sonic excitation at the fluid-solid interface[6]. An important consideration when predicting transition is that superposition of the factors which influence it is not possible, and in each flow case, the dominant effects must be isolated.

TABLE 1. FACTORS INFLUENCING TRANSITION

Factor	Transition Promoted By
Free stream turbulence	Increasing
Pressure gradient	Positive
Roughness	Increasing
Heat transfer	Heating
Surface curvature	Increasing (concave)

The above discussion points to the fact that the mechanisms governing transition are indeed delicate and that the external energy involved to promote or postpone transition is small compared to that required to maintain the basic flow. This observation in conjunction with the theory of laminar-boundary-layer oscillations forms the basis for the following thesis. Boundary-layer transition may possibly be influenced by an electrical perturbation of the proper intensity, frequency, and wavelength. This thesis is developed in relation to the effects of corona discharge on the boundary-layer transition of steady-state incompressible air flow over a flat plate.

THEORY OF BOUNDARY-LAYER OSCILLATIONS

Boundary-layer stability theory, as ultimately developed by Tollmein and Schlichting, is based on a method of small disturbances which is characterized by the following premises.

(1) Laminar flow is affected by small disturbances.

(2) The disturbances are initially random in nature and are inherent in the flow, by virtue of free stream turbulence, or boundary surface conditions.

(3) If the disturbances decrease with time, the flow will remain stable and laminar.

(4) If the disturbances grow with time, the flow will become unstable with the possibility of transition to turbulence.

(5) A critical Reynolds Number exists below which no disturbances will be amplified.

The main lines of the theory of stability are outlined in Schlichting's text[7] and discussed by Schubauer and Skramstad in Reference 5. The discussion given here draws upon both of these works.

In describing the turbulent or nonturbulent stream, the velocity and pressure are separated into a mean value component and an oscillating component. Instantaneous velocity and pressure values are represented as the sum of the two components. The mean value

components are generally defined with respect to time at a fixed point in space. Due to the statistical nature of turbulence, they may also be averaged at different points in space at the same time. The total velocity components and pressure are then given by the following:

$$u = U + u' \tag{1}$$

$$v = V + v' \tag{2}$$

$$w = W + w' \tag{3}$$

$$p = P + p' \tag{4}$$

where capitals denote the mean values and primes the fluctuating values. Two-dimensional mean flow with two-dimensional disturbances is considered. Schlichting and Schubauer note that this is the conservative case in that analysis of three-dimensional disturbances will give higher critical Reynolds Numbers. Simplifications are introduced by stating that $V = 0$ everywhere and, in the boundary layer, the mean flow is only a function of distance from the surface, y. Thus, we have

$$U = f(y) \tag{5}$$

$$V = 0 \tag{6}$$

$$w = 0 \tag{7}$$

$$u' = u'(x,y,t) \tag{8}$$

$$v' = v'(x,y,t) \tag{9}$$

$$p' = p'(x,y,t). \tag{10}$$

It is assumed that both the total motion, given by Equations 1 through 3, and the mean motion are solutions of the Navier-Stokes equations. Substituting Equations 1 through 3 in the Navier-Stokes equations gives

the following two equations after squares and products of disturbance velocities and of their differential coefficients are neglected.

$$\frac{\partial u'}{\partial t} + U\frac{\partial u'}{\partial x} + v'\frac{\partial U}{\partial y} = \nu\left(\frac{\partial^2 U}{\partial y^2} + \nabla^2 u'\right) - \frac{1}{\rho}\left(\frac{\partial P}{\partial x} + \frac{\partial p'}{\partial x}\right) . \qquad (11)$$

$$\frac{\partial v'}{\partial t} + U\frac{\partial v'}{\partial x} = \nu\nabla^2 v' - \frac{1}{\rho}\left(\frac{\partial P}{\partial y} + \frac{\partial p'}{\partial y}\right) . \qquad (12)$$

The continuity equation for the disturbances is

$$\frac{\partial u'}{\partial x} + \frac{\partial v'}{\partial y} = 0. \qquad (13)$$

Since the mean flow satisfies the Navier-Stokes equation, two more relations are gained by letting $u' = v' = p' = 0$ in Equations 11 and 12.

$$0 = \nu\frac{\partial^2 U}{\partial y^2} - \frac{1}{\rho}\left(\frac{\partial P}{\partial x}\right) . \qquad (14)$$

$$0 = -\frac{1}{\rho}\left(\frac{\partial P}{\partial y}\right) . \qquad (15)$$

Subtracting from Equations 11 and 12, respectively, Equations 13 and 14, gives expressions solely in terms of U and the disturbances.

$$\frac{\partial u'}{\partial t} + U\frac{\partial u'}{\partial x} + v'\frac{\partial U}{\partial y} = \nu\nabla^2 u' - \frac{1}{\rho}\frac{\partial p'}{\partial x} . \qquad (16)$$

$$\frac{\partial v'}{\partial t} + U\frac{\partial v'}{\partial x} = \nu\nabla^2 v' - \frac{1}{\rho}\frac{\partial p'}{\partial y} . \qquad (17)$$

Equations 16 and 17 are the fundamental hydrodynamic equations for small disturbances. These equations may be subtracted to eliminate

the pressure disturbance, after selective differentiation, yielding, together with the continuity equation, two equations for u' and v'.

The mathematical form of the disturbance is suggested by the nature of the oscillations. Observing the oscillations at a fixed point suggests the passage of a traveling wave in the boundary layer. Thus, the disturbance is periodic and may, therefore, be represented by a Fourier series and investigated using a single term of the series. A stream function, ψ, which satisfies this condition is

$$\psi = F(y) \exp[i(\alpha x - \beta t)] \ . \tag{18}$$

The amplitude of the stream function, F, is represented by F(y). Since the mean flow depends solely on y, the amplitude is also assumed to depend on y only. The wavelength is given by

$$\lambda = 2\pi/\alpha \ , \tag{19}$$

and the frequency and amplification are given by β. The quantity β is complex

$$\beta = \beta_r + i\beta_i \ , \tag{20}$$

where β_r is the circular frequency or $2\pi f$, and β_i is the amplification coefficient. By substituting Equation 20 in Equation 18, it is seen that the disturbances grow with time if β_i is greater than zero. The wave velocity, c_r, is then

$$c_r = f\lambda = \left(\frac{\beta_r}{2\pi}\right)\left(\frac{2\pi}{\alpha}\right) = \frac{\beta_r}{\alpha} \ . \tag{21}$$

The stream function gives the disturbance velocities as follows:

$$u' = \frac{\partial \psi}{\partial y} , \tag{22}$$

$$v' = - \frac{\partial \psi}{\partial x} . \tag{23}$$

Thus

$$u' = F' \exp[i(\alpha x - \beta t)] , \tag{24}$$

$$v' = - i\alpha F \exp[i(\alpha x - \beta t)] , \tag{25}$$

where the prime on F denotes differentiation with respect to y.

It is immediately seen that the continuity equation is satisfied. After p' is eliminated from Equations 16 and 17, the disturbance velocities are introduced and the resulting equation is nondimensionalized with respect to the maximum free stream velocity, U_m, and the boundary-layer thickness, δ. The resulting fourth order nonlinear equation, the Orr-Sommerfeld equation, is called the stability equation.

$$(U-c)(F'' - \alpha^2 F) - U''F = \frac{- i}{\alpha Re_\delta} (F'''' - 2\alpha^2 F'' + \alpha^4 F) . \tag{26}$$

Here

$$c = \frac{\beta}{\alpha} = c_r + i\, c_i ,$$

$$Re_\delta = \frac{U_m \delta}{\nu} .$$

The terms on the left side of the equation represent inertial terms and those on the right side viscous terms. For large Reynolds Number, the viscous terms are neglected and the resulting equation is known as the frictionless stability equation. The boundary conditions applicable to Equation 26 demand that the components of the turbulent velocity be zero at the wall and at a large distance from it. These boundary conditions are the following:

$$\text{At } y = 0 \text{ and } y = \infty;$$

$$u' = v' = F = F' = 0.$$

If the frictionless stability equation is investigated, only two of the above boundary conditions may be satisfied.

A general solution of Equation 26 may be formed with four particular solutions. The form of the particular solutions depends on the form of the boundary-layer velocity profile. Both Tollmein and Schlichting obtained solutions for profiles closely approximating a Blasius distribution. The solutions reduce to an eigen-value problem in terms of the parameters α, Re_δ, and c. For each α and R_e value, one complex eigen-value, c, is found. The locus of points where c_i, or essentially β_i, equals zero is the curve of neutral stability. Enclosed by this curve are unstable solutions. Theoretical wave parameters for neutral oscillations taken directly from Schlichting are given below in Table 2. Here Re is based on the displacement thickness, δ^*. Using the tabulated values, Schlichting's neutral disturbance curve is plotted in terms of frequency, wavelength, and velocity in Figures 1 through 3.

TABLE 2. NEUTRAL-STABILITY CURVE

	Branch I			Branch II		
$\frac{c_r}{U_m}$	R_δ^*	$\alpha\delta^*$	$\frac{\beta_r \nu}{U_m^2} \times 10^6$	R_δ^*	$\alpha\delta^*$	$\frac{\beta_r \nu}{U_m^2} \times 10^6$
0.200	7200	0.077	2.14	37,600	0.149	0.70
0.250	3010	0.101	8.39	12,000	0.188	3.92
0.300	1530	0.129	25.3	4,640	0.223	14.4
0.325	1150	0.143	40.4	3,290	0.238	23.5
0.350	893	0.159	62.3	2,070	0.251	42.4
0.375	736	0.181	92.2	1,420	0.264	69.7
0.400	633	0.205	129.5	1,020	0.274	107.4
0.420	606	0.239	165.7	713	0.273	161.0

The above solution for neutral oscillations was based on the assumption that $U = f(y)$ and $V = 0$ in the boundary layer. This is equivalent to assuming a nonthickening boundary layer. Since the boundary layer grows in thickness in the downstream direction, the validity of the solution may be questioned on physical grounds. This is one of the basic criticisms of stability theory. However, the dependence of U on y is large, compared to the dependence on x, and V is small compared with U. The experimental work of Schubauer and Skramstad (1947) qualitatively confirmed the general characteristics predicted by the theory. This is illustrated in Figure 1 where, along with Schlichting's neutral-stability curve, are plotted experimental data points generated by Schubauer and Skramstad. The qualitative differences are partially explained by the fact that the values of δ^* used by Schubauer and Skramstad are calculated for a thickening boundary layer and increase with x. Following a different procedure, developed by C. C. Lin[8], Shen repeated the calculations for the neutral-stability curve and obtained results in closer agreement with experiment. Shen's curve is also shown in Figure 1.

For the present investigation, the range of Re_{δ^*} is sufficiently high that Schlichting's results are quantitatively satisfactory. Realizing this fact, the values of δ^* may be related to x with minimal compromise of theory to experiment. For convenience, the Reynolds Number based on δ^* is converted to Re_x using the following relation,

$$\delta^* = 1.72 \left(\frac{\nu x}{U_m}\right)^{1/2}, \qquad (27)$$

from Reference 5.

Together with

$$Re_x = \frac{U_m x}{\nu} , \quad \text{and}$$

$$Re_{\delta^*} = \frac{U_m \delta^*}{\nu} , \quad \text{this gives}$$

$$Re_x = \left(\frac{Re_{\delta^*}}{1.72}\right)^2 . \tag{28}$$

Equation 28 was used to replot Figures 1 through 3 based on Re_x instead of Re_{δ^*}. The resulting curves are presented in Figures 4, 5, and 6 where β_r and α have been replaced by f and λ, respectively.

Disturbances that enter or originate within the bounds of the neutral-stability curve are amplified. This amplification process is the link between instability and transition. The amplification of the disturbance may be expressed as the ratio of the amplitudes at two discrete times. From Equation 18, the amplitude ratio at two consecutive crests, on a given streamline, is

$$\frac{A_2}{A_1} = \exp(\beta_i t_2)/\exp(\beta_i t_1) , \tag{29}$$

or

$$\frac{A_2}{A_1} = \exp\int_{t_1}^{t_2} \beta_i \, dt , \tag{30}$$

where A_1 is the amplitude at t_1 and A_2 is the amplitude at t_2. As pointed out by Gyorgyfalvy[9], transition can be predicted empirically based on the integrated amplification rate. According to this

criterion, transition occurs after the onset of instability when

$$\int_{t_1}^{t_{tr}} \beta_i \, dt = 9. \qquad (31)$$

For disturbances entering at Branch I of the neutral-stability curve, Figure 1, this integrated amplification is first reached at $Re_x = 3.1 \times 10^6$. This is in good agreement with experimental values for transition on a flat plate with zero pressure gradient for the condition of free stream turbulence intensity less than 0.1, Reference 5.

The theory of boundary-layer oscillations described above forms the basis for this experimental investigation. If the necessary condition for the occurrence of transition is the amplification of boundary-layer disturbances, then the disruption of this amplification process may be expected to retard transition. The possibility of accomplishing this with controlled-frequency electrical disturbances is described in the following section.

ELECTRICAL PERTURBATIONS

The sensitive phenomenon of transition may be influenced by mechanical disturbances with relatively small amounts of input energy required. This is illustrated in References 5 and 6 which describe the effects of loudspeakers on flow transition. In addition to such sonic interference investigations, Deimen and Clark[10] have experimentally studied the effect of replacing a section of a solid flow boundary with a vibrating membrane. All of the above efforts have demonstrated that transition may be promoted by mechanical disturbances of the proper frequency. The question exists as to what other forms of disturbance may influence transition and is it possible to forestall it.

For years it has been known that electric fields and the presence of ions effect fluid properties and performance.[11] A dramatic illustration of the capability of corona discharge to influence boundary-layer phenomena is given in Reference 12. This work describes the interaction of a corona point discharge with a free-convection boundary layer on a vertical plate. Significantly, large changes in heat-transfer coefficient, local fourfold increases in some cases, were obtainable with corona power expenditures of less than 1 watt. A recent experimental investigation[13] has demonstrated that flow attachment may also be influenced by corona wind. Based on this knowledge, one may conjecture that electrical disturbances may be capable of influencing transition. For this study, the corona discharge was chosen as the disturbance or perturbation mechanism.

Corona discharge is usually viewed as undesirable. When speaking of high-voltage electrical equipment and power transmission, this view is well taken. As pointed out by AIEE engineers[14], corona power loss of 3 kw per mile on high-voltage transmission lines, with accompanying insulation deterioration, is not uncommon. However, many uses of corona have been discovered with beneficial results. Several applications are air-pollution control, radiation detection, and static elimination. The study of corona discharge has also served science in helping to explain processes of electrical breakdown in gases. It was the positive-point corona which led physicists to the discovery of the role of photoionization in gases. A description of the corona discharge and its application to the experiment follows.

Corona, as defined by Loeb, is the expression used to describe the class of luminous phenomena associated with the current jump at a highly stressed electrode preceding a spark breakdown of the gap. Associated with corona breakdown is an electrode of small radius or high curvature. If such an electrode is placed near one of low curvature, the electric field induced is asymmetric and extremely concentrated at the highly curved electrode. As the potential difference between the electrodes is raised, ionization of the air in the immediate vicinity of the highly curved electrode occurs; however, no spark crosses the gap because the field is too low farther from the curved electrode. The resulting corona discharge will be of positive or negative character depending upon the electrode polarity.[15]

If the highly curved electrode or wire has a negative potential, the positive ions formed near the wire will acquire relatively high energy from the field and essentially bombard the cathode wire. These positive ions, while forming a space charge near the cathode which gives the negative corona its fluctuating characteristic, will produce the necessary electrons to sustain the discharge. On the other hand, the electrons that are formed will migrate relatively slowly to the anode because of the reduction in field strength away from the wire. These electrons will generally not have enough energy to cause further ionization and may be expected to attach themselves to neutral molecules of electro-negative gases forming large, even slower moving, ions. A wire of positive potential will attract the ionized electrons with great intensity causing electron avalanches toward the wire. This liberates a positive ion space charge which drifts toward the cathode sustaining the discharge although reducing the field at the wire.

Positive wire corona was chosen for the investigation because of the more uniform nature of the discharge. It was feared that the nonperiodic pulsating nature of a negative wire corona[16] might detrimentally effect the flow due to noise in addition to adding an uncontrolled variable to the experiment. Qualitatively, some relations between the corona variables are given in Table 3.

TABLE 3. CORONA VARIABLES

Variable	Effect of Variable Increase on Corona Current
Gap potential	Increase
Anode curvature	Increase
Gap spacing	Decrease
Density	Decrease

Once liberated, the negatively charged bodies, whether in the form of electrons or molecules, will experience a body force due to the presence of the electric field. This body force will, in effect, be distributed throughout the fluid between the electrodes by virtue of electron-molecule and ion-molecule collisions. In this respect, the electrical disturbance is physically different from the mechanical disturbances mentioned above.

A corona discharge with a controlled frequency component was employed with the aim of stabilizing the boundary layer as described in the following section. Positive ions were used to interact with the boundary-layer flow.

EXPERIMENTAL INVESTIGATION

DESIGN OF THE EXPERIMENT

In attempting to interact the corona discharge with the boundary-layer instabilities, an essential feature of the experimental investigation is the manner in which the electrical disturbance is applied to the boundary-layer flow. Several desirable characteristics are:

(1) The disturbance shall incorporate a pulsating controlled-frequency component.

(2) The mechanism for applying the disturbance shall not trip the boundary layer by virtue of its presence.

(3) The disturbance shall cover a relatively large area of the flow field.

A series of corona wires, suspended outside the boundary layer, parallel to the flow surface and normal to the flow direction, appears to satisfy these requirements.

Several variables are of prime importance. These are, the disturbance frequency and intensity and the spacing and location of the wires in the flow direction. Because the amplification of boundary-layer oscillations is a selective process, depending on frequency, it would seem that the predominant variable of the disturbance should be the disturbance frequency. However, since the boundary-layer oscillations are in the form of waves, one might expect that any disturbance

which could interact with the oscillations would also have wavelike characteristics. This leads to the idea of adjusting the corona wire spacing to be a multiple of the wavelength which is possessed by a predominant boundary-layer oscillation. The provision for attaining this spacing is described in a later section along with the electrical equipment which controls the corona frequency and intensity.

The existence of predominant oscillations has been theorized by Schlichting and demonstrated by Schubauer and Skramstad, Reference 5, and Deimen and Clark, Reference 10. Such oscillations obtain because of the nature of the amplification process. Referring to Figure 4, waves of many frequencies enter the amplification zone through Branch I and are then amplified at a rate dependent on their frequency. They then proceed to the value of Re_x at which an observation is made. Initial oscillations are supposedly present in the boundary layer at all values of Re_x and, therefore, enter the diagram at all points. It is obvious from Equation 30 that oscillations which enter at Branch I and proceed to Branch II will receive the highest amplification. When an observation is made at a specific value of Re_x, there exists one value of $\beta_r \nu / U_m^2$ which will be more highly amplified than any other. This is the predominant oscillation. The question that remains is where on the diagram is the locus of the predominant, or most amplified, oscillations. This can be determined by considering the initial energy distribution of the oscillations and the damping prior to reaching Branch I of the neutral-stability curve[5]. The desired locus of points lies in the amplification zone near Branch II. Knowing this,

the corona discharge frequency and wire spacing may be gauged to match the predominant oscillations.

Further details concerning the design of the experiment and apparatus are described in the section below.

EXPERIMENTAL APPARATUS

The experimental apparatus for this transition study was selected or designed to yield the following test conditions:

Boundary surface - flat with zero pressure gradient, electrical conductor

Flow conditions - steady-state, incompressible flow of air

Transition detector - reliable, rapid nonconductor

Electrical equipment - high voltage, low current, controlled frequency pulsation.

Boundary Surface

The boundary surface was a 3-foot-wide by 6-foot-long flat plate consisting of a thin sheet of aluminum laminated to a 3/4-inch-thick sheet of A-A exterior grade plywood. The aluminum was 3003 H14 cold-rolled sheet 1/32-inch thick and 36 inches wide. Surface roughness values for such cold-rolled products typically range from 10 to 20 microinches, rms. Special care was taken to keep the plate surface scratch-free and clean. Waviness was imperceptible even when viewed near grazing incidence; however, some slight sag was present as revealed

by a crack of light showing beneath a straight edge placed on the plate normal to the flow direction. A straight edge placed parallel to the flow direction revealed no cracks of light.

The leading edge of the plate was a 15-degree bevel. Initially, the bevel nose was rounded; however, early test results led to the subsequent application of a sharp builtup nose. This is described in the testing section. Full-scale drawings of both leading edge shapes appear in Figure 7. Three rows of holes for static pressure taps were placed in the plate surface to allow determination of pressure gradients on the plate. A layout of the holes and a section view of a pressure tap is shown in Figure 8. A curved aluminum flap was attached to the trailing edge of the plate to maintain the flow blockage necessary for keeping the stagnation point on the active side of the plate. This flap may be seen in Figures 9 and 10.

The plate was mounted horizontally at mid-height in the flow channel test section with the active side facing downward. Steel angles were used to secure the plate in the test section with a minimum of flow interference, Figure 11. Slots in the larger angles allowed the plate to be inclined to the flow. No vibration of the plate was visible during testing.

Flow Channel

The flow channel used for this experimental investigation is Battelle Memorial Institute's subsonic wind tunnel, the general layout of which is shown in Figure 12. The tunnel is an open-circuit, or

"NPL" type which draws in fresh outside air continuously. From the settling chamber to the test section, the area reduction is approximately 10:1. A 125-hp induction motor drives the fan at 700 rpm. The fan (Figure 13) is a Hartzell No. MP-96-6 with a diameter of 8 feet and adjustable pitch blades. All testing was done with a blade pitch of 17 degrees. The velocity profile across the tunnel test section is flat. This can be seen from a typical plot of dynamic pressure ratio versus distance, Figure 14. In the test section, the wall boundary layer is turbulent and several inches thick. See Figure 15.

The level of turbulence in the test section is low, as governed by three 24-mesh screens, of 0.0075-inch wire, installed at the entrance to the settling chamber. The projected open area of the screens is 67.4 percent. Figures 16 and 17 show the tunnel mouth and turbulence screens. The method employed to measure the turbulence made use of a 5-inch-diameter "pressure sphere". Pressure sphere measurements yield the turbulence factor which is defined as the ratio of an effective Reynolds Number to the actual Reynolds Number. For turbulence factors less than 2, the percent turbulence is related by the following expression[18].

$$\text{Percent turbulence} = 1.25\ (\text{turbulence factor}-1). \tag{32}$$

$$\text{Percent turbulence} = \left[(u')^2 + (v')^2 + (w')^2\right]^{1/2} \times 100/U_{in}. \tag{33}$$

At a flow speed of 140 fps, pressure sphere determinations yielded a turbulence factor of 1.083.* This relates to a turbulence intensity of 0.10 percent. In general, the turbulence level increases with tunnel test velocity.

Transition Detector

Many methods may be used to detect the locations of the transition region. Some of the most common include the following:

(1) Measuring or plotting the velocity profile in the boundary layer and determining whether the flow is laminar or turbulent by the profile's shape.

(2) Reading the dynamic pressure at a small height above the surface and noting the distance from the leading edge where it is a minimum.

(3) Reading the dynamic pressure as in (2), or velocity, with a hot-wire anemometer, and noting unsteady or oscillating values.

(4) Emitting smoke from the surface and noting the point where the smoke is dispersed.

---

* Personal communication with V. O. Hoehne, Battelle Memorial Institute, Columbus, Ohio.

(5) Coating the flow surface with evaporating chemicals. Where the flow is turbulent, the evaporation will proceed most rapidly.

(6) Listening to a total head probe with a stethoscope as the probe is moved along the flow surface. A laminable flow makes a hissing sound while a roar is heard when the flow is turbulent.

A near-surface impact pressure probe was used to detect transition, making use of Methods (2) and (3) above. This method was chosen because it is simple, rapid, visual, and amenable to data recording.

If an impact pressure probe is traversed along the flow surface, in the flow direction, the reading, which is directly proportional to the square of the local velocity, is determined by the thickness of the boundary layer, the height of the probe above the surface, and the shape of the local velocity profile. As the probe moves away from the leading edge, at a fixed distance from the surface, the laminar boundary layer thickens, effectively moving the probe into regions of lower velocity. However, once the turbulent zone is reached, the velocity profile changes, causing an abrupt increase in local velocity and dynamic pressure. As the probe continues moving rearward in the turbulent region, the dynamic pressure again decreases due to the thickening of the turbulent boundary layer. This sequence of events is illustrated in Figure 18. No definite, fixed transition

point exists. The start of the transition region is taken as the minimum point on the curve, Point (a). Additionally, this point is marked experimentally by oscillations in velocity readings because of the unsteady nature of the transition process.

A motorized probe was designed to traverse the underside of the plate in the longitudinal direction. The probe boom, a 1-1/4-inch-square aluminum extrusion, was suspended and pivoted on a crossbar downstream of the plate and test section. The crossbar penetrated the wind tunnel walls and was isolated from tunnel structure vibrations. A sprocket-and-chain drive was employed capable of moving the boom at a rate of 10 inches per minute. The probe mechanism may be seen in Figures 9 and 10. At the forward end of the boom, an offset steel tube accepted the glass probe used for the measurements. The glass portion of the probe was connected directly to a pressure line which ran through the boom and lead out of the tunnel.

Figure 19 shows a typical glass probe insert. The glass probe tip could be sized to virtually any length and diameter by suitable torch heating and drawing. Tip diameters ranging from 0.010 to 0.050 inch were used in the experiment. The tip ends were ground flat using a small croakus cloth wheel in an electric drill. In Figure 20, the probe offset and glass insert are shown in relation to the plate surface. The offset was adjusted to maintain the glass tip tangent to the plate at all times.

Electrical Equipment

A controlled frequency pulsating potential was applied to a series of corona wires suspended over the flat plate. The wires were suspended and tightened by means of a double row of screws which were installed in plexiglass strips, Figures 20 and 21, secured to the underside of the plate-support angles. Within the test section, all exposed conductors were grounded with the exception of the corona wires and rows of screws. Several types of corona wires were tried during the course of the experiment. Ultimately, the wire most resistant to breaking proved to be 0.008-inch steel model airplane control wire. Music wire of 0.004-inch and 0.011-inch diameter proved to be unsatisfactory.

A pulsating potential was applied to the wires by direct superposition of an alternating voltage signal on a steady d-c voltage. This input form is illustrated in Figure 22. The superposition was employed because of the difficulty and expense involved in obtaining or designing equipment to yield a pulsating signal having a potential level as high as the d-c level. A circuit diagram appears in Figure 23. The components of the electrical apparatus may be seen in Figure 24 and are specified below.

Oscillator - Hewlett-Packard wide-range oscillator, Model 200 CD. This generates the variable frequency component of the corona potential.

Amplifier - Scott, 100-watt, laboratory power amplifier, Type 265A.
The amplifier boosts the oscillator output for input to the stepup transformer.

Transformer - Merit, 25-watt, audio frequency transformer, Model A-3129.
This transformer was run "backwards" to gain the maximum voltage stepup possible.

High Voltage D-C Power Supply - Custom designed for Battelle Memorial Institute.
Maximum output - 14,000 volts, ripple-free.

Voltage Divider - Voltage split of 50,000:1, total resistance of 50 million ohms.
Used in conjunction with oscillograph for voltage measurement.

Scope - Dumont oscillograph, Model 304A.
Used to measure and visualize imposed voltage.

Ammeter - Simpson, Model 374 microammeter.
Used to measure average corona current.

The performance of the electrical system varied with the size and number of corona wires used. Normally, four 0.008-inch wires were used, each 36 inches long. With such a load, the maximum d-c output attainable was 12,000 volts. The maximum peak-to-peak fluctuating voltage attainable was a function of frequency and varied from almost nothing at 1 cps to 4000 volts at 6000 cps.

EXPERIMENTAL PROCEDURE

Before proceeding with transition tests, the static pressure distribution over the surface of the plate was checked, in the presence of the traversing pressure probe, at several flow speeds. The surface pressure taps (see Figure 8) were connected to the manometer board shown in Figure 25. Each U-tube contained Merriam Red Oil, specific gravity 0.827, and was open to the atmosphere on one side. The column height could be read conveniently to 0.05 inch which is the limit of accuracy for simple manometers. Both legs of the U-tube were read simultaneously. Generally, the static pressure readings were within 0.1 inch of the average of the readings, the maximum deviation being less than two percent of the total dynamic head. Figure 26 presents one set of typical test data for the static pressure distribution over the plate. The static pressure readings were recorded at the beginning of each test and remained constant throughout the test for a given speed setting.

For the transition tests, the experimental procedure is outlined below.

(1) The desired tunnel speed was set approximately. When equilibrium temperature and flow conditions were reached, the speed was set more accurately.

(2) Transition was probed for using the traversing pressure probe.

(3) The desired corona wires were installed followed by a reprobe for transition detection.

(4) The corona discharge was activated followed by a third probe for transition detection.

Details relating to Parts (1) through (4) of the experimental procedure are described in the section entitled, RESULTS OF EXPERIMENTAL INVESTIGATION. Some of the experimental calculations which were required to perform the tests are presented in the following paragraphs.

EXPERIMENTAL CALCULATIONS

To perform the transition tests required determination of the following quantities:

(1) Air density.

(2) Flow speed.

(3) Local Reynolds Number.

(4) Frequency and wavelength of predominant boundary-layer oscillations.

Air Density

It is necessary to know the air density to calculate the flow speed and the local Reynolds Number. The tests were conducted at flow speeds of approximately 150 to 200 fps at temperatures close to 30 degrees F. Corresponding Mach Numbers are less than 0.2, classifying the flow as subsonic and incompressible. The air density is given by the equation of state for a perfect gas.

$$\rho = \frac{p}{RT} \quad . \tag{34}$$

For convenience, the pressure is left in barometric units. The absolute pressure, p_a, is determined by subtracting the local static pressure near the plate from the barometric pressure.

$$\rho\left(\frac{lb_m}{ft^3}\right) = \frac{p_a(\text{in. hg}) \times 70.8(lb/ft^2/\text{in. hg})}{53.3(ft\text{-}lb_f/lb_m\text{-}°R) \times T(°R)} = 1.33\ \frac{p_a}{T} \quad . \tag{35}$$

The air temperature within the test section is displayed at the tunnel control console.

Flow Speed

The test section flow speed is calculated by applying an experimentally determined correction factor to Bernoulli's equation. Bernoulli's equation is

$$p + \frac{\rho\ U_m^2}{2} = \text{constant} \quad . \tag{36}$$

By assuming zero velocity in the settling chamber, this gives

$$h_q = \frac{\rho\ U_m^2}{2} \quad , \tag{37}$$

where h_q is the difference in static pressure across the inlet contraction. Both h_q and the static pressure near the entrance to the test section, h_s, are displayed at the tunnel control consol manometers, Figure 27. The flow speed correction factor accounts for

boundary-layer growth, frictional effects and settling chamber velocity. Using total head probes, the correction factor for the Battelle wind tunnel has been found to be 1.01. Thus, Equation 37 is inverted and corrected to read,

$$U_m = 1.01 \left(\frac{2\, h_q}{\rho}\right)^{1/2} . \qquad (38)$$

In terms of the direct reading, h_q, this becomes

$$U_m\left(\frac{ft}{sec}\right) = \frac{1.01}{\rho}\left[2 \times h_q(\text{in. oil}) \times 4.32\left(\frac{lb_f/ft^2}{\text{in. oil}}\right) \times 32.17\left(\frac{lb_m\text{-ft}}{lb_f\text{-sec}^2}\right)\right]^{1/2},$$

or

$$U_m = 16.85 \left(\frac{h_q}{\rho}\right)^{1/2} . \qquad (39)$$

The tunnel head, h_q, was varied by adjusting the position of the air-intake ports shown in Figure 28. These openings are approximately 8 feet upstream of the fan.

Local Reynolds Number

The local Reynolds Number is defined in terms of the distance from the leading edge of the plate.

$$Re = \rho\frac{U_m\, x}{\mu} . \qquad (40)$$

The only unprescribed quantity in Equation 40 is the viscosity μ. The viscosity was considered to be a function of temperature only. A linear variation, prescribed by the following points, used[19].

Air Viscosity, $lb_m/ft\text{-}sec$	Temperature, °F
1.110×10^{-5}	0
1.285×10^{-5}	100

Frequency and Wavelength of Boundary-Layer Oscillation

The amplification characteristics of boundary-layer oscillations are presented in Figures 4 and 5 in terms of Re_x and the frequency and wavelength parameters $f\nu/U_m^2$ and λ/δ^*, respectively. At a given Reynolds Number, it is desired to know the specific wave characteristics for selected points on the diagram. The frequency is obtained directly by multiplying the values $f\nu/U_m^2$ by U_m^2/ν. Equation 35 is used to obtain the kinematic viscosity. The wavelength is determined from the dimensions parameter λ/δ^* by using Equation 27 to find δ^*.

RESULTS OF EXPERIMENTAL INVESTIGATION

The experimental investigation may best be described by three categories of chronological effort:

(1) Tests and modifications to obtain the necessary laminar boundary layer on the plate.

(2) Tests and modifications to enable the detection of transition.

(3) Tests and modifications to determine the effects of corona discharge on transition.

An account of these tests and results constitutes the remainder of this section.

OBTAINING A LAMINAR BOUNDARY LAYER

A flow region with an associated, stable laminar boundary layer is mandatory for investigating transition phenomena. Several tests were run before it was determined that such a flow region did not exist with the initial leading edge geometry shown in Figure 7a. The traversing pressure probe was used with glass tip diameters of 0.01 inch and 0.04 inch at several flow speeds. Traverses were conducted along the plate centerline moving from the rear of the plate toward the leading edge. The pressure-distance pattern shown in Figure 18 was sought. The pressure dip, or pressure fluctuation, signaling the onset of transition was expected to occur between 1 and 2 feet from the leading edge. Instead, pressure fluctuations were

observed several inches from the leading edge. Further back from the leading edge, no transition could be detected. Data illustrating these fluctuations are presented in Figure 29 for three different tests. The erratic pressure distributions near the leading edge indicated the presence of premature transition, or possibly separation.

At this point it was decided to modify the leading edge because it was felt that the rounded shape was causing the irregular flow. A sharp edge was modeled onto the existing nose section using a polyester base automobile body putty, Figure 7b. The final surface finish was obtained by alternately buffing with triple-zero wet paper and spraying with silver paint. The surface change from the painted edge to the aluminum was visually apparent but barely perceptible to the fingertips. With a new glass probe installed, 0.042-inch diameter, several tests were performed to again seek the transition impact pressure pattern. In Tests 5 and 6 , the plate was tilted to slight positive and negative angles of attack. Tilting the plate caused a perceptible change in the static pressure distribution in the flow direction, showing a negative gradient for + 1/2-degree angle of attack and a positive gradient for - 1/2-degree angle of attack. However, in all cases, the irregular impact pressure pattern near the nose was still present. Figure 30 displays the pressure profiles for the three tests with the sharp leading edge.

It is believed that the severe dips in impact pressure shown in Figure 30 are caused by boundary-layer separation at the sharp leading edge. If the surface probe was within a separation bubble, the

local velocity might well be directed opposite to the flow direction due to eddying. This would explain the severe pressure dips. Such separation would be caused if the flow stagnation point rested on the inclined edge of the nose rather than at the top. The flow would then have to turn abruptly around the sharp leading edge in order to pass to the active side of the plate.

Another modification of the plate was then undertaken to remedy this condition. A curved aluminum flap was secured to the trailing edge of the plate as shown in Figures 9 and 10. This proved to be the solution, for the irregular pressure pattern near the leading edge was no longer present. Test data confirming this fact are also presented in Figure 30. It is believed that the flap provided sufficient blockage between the active surface of the plate and the test section floor to force the impinging streamlines to curve upward when approaching the plate, thus forcing the stagnation point to the active side of the plate. The presence of the flap did not distort the static pressure distribution. This concludes the description of the test efforts concerned with obtaining a laminar boundary layer.

DETECTING TRANSITION

Although Test 7 (Figure 30) verified the existence of a smooth boundary-layer development, it did not indicate the presence of transition. Another test was conducted with the same 0.042-in.-diameter probe at a flow speed of 165 fps. No transition was

detected. The glass probe was replaced with one having an external tip diameter of 0.022 inch with a 0.011-inch hole. Using this probe impact pressure, fluctuations were observed in the next test, Test 8, at 1.65 feet from the leading edge. Figure 31 shows the pressure profile with the extreme value of pressure fluctuation plotted at 1.65 feet. The pressure fluctuations were persistent with a peaking frequency of approximately once per second. The distance from the leading edge where these fluctuations were encountered was taken as the starting point for transition. All subsequent tests were conducted with a probe tip diameter equal to 0.022 inch.

Following Test 8, in which transition was detected, the traversing impact pressure probe was "balanced" against a fixed impact pressure probe. The fixed probe was mounted as shown in Figure 32. This was done in order to partially eliminate the effects of tunnel gusts on windy days. Test 9 was run at 164 fps. Transition was detected at 1.5 feet from the leading edge. The impact pressure profile is also shown in Figure 31. Associated with Tests 8 and 9 are the following transition Reynolds Numbers:

$$\text{Test 8, } Re_{xtr} = 1.66 \times 10^6.$$

$$\text{Test 9, } Re_{xtr} = 1.54 \times 10^6.$$

According to hot-wire studies performed for a flat plate with zero pressure gradient (Reference 5), the free stream turbulence intensity associated with the above transitions is about 0.3 percent. Although quite low, this value is three times the 0.1 percent value quoted

earlier for a 140 fps flow speed. Possibly the sensitivity of the pressure sphere technique for detecting extremely low turbulence levels is not sufficient.

At this time, it was desired to confirm the presence of transition before undertaking the corona tests. A visualization technique was tried in which a subliming solid is used to coat the surface of the plate. In the turbulent region, the solid will sublime first, leaving a visual pattern of transition. Solutions of alcohol, saturated with both naphthalene and biphenyl, were used. After application of the solution, the alcohol evaporated leaving the surface coated with fine white crystals. The sublimation temperature of both chemicals is close to 70 degrees F. A test was conducted with each chemical at an ambient temperature of approximately 55 degrees F. In both cases, the crystals failed to sublime preferentially. Instead, much of the coated strip remained, even at the conclusion of the test. The air temperature was obviously too low to allow valid use of this technique.

An analytical correlation was used to verify the presence of transition. The basis of the correlation is as follows: At a given distance from the leading edge and from the plate surface, the ratio of local velocity to free stream velocity may be computed from the impact pressure probe reading. This velocity may be compared to those expected for laminar and turbulent velocity profiles at the particular point of measurement.

The local velocity ratio, U/U_m, is equal to the square root of the local dynamic pressure ratio.

$$\frac{U}{U_m} = \left(\frac{\text{Full impact pressure - local impact pressure}}{\text{Full impact pressure}}\right)^{1/2}. \quad (41)$$

The thickness of local laminar and turbulent boundary layers is given in Reference 7 for growth starting at the leading edge.

$$\delta_L = 5 \left(\frac{\nu x}{U_m}\right)^{1/2}. \quad (42)$$

$$\delta_T = 0.37 \times \left(\frac{\nu}{U_m x}\right)^{1/5}. \quad (43)$$

For the laminar flow, the local velocity at a given distance from the surface is computed using the similarity parameter, η.

$$\eta = 5 \left(y_{effective}/\delta_L\right). \quad (44)$$

The parameter, η, is related to the laminar velocity ratio, $(U/U_m)_L$, as tabulated below.

TABLE 4. VELOCITY RATIOS FOR A LAMINAR BOUNDARY LAYER ALONG A FLAT PLATE[5]

η	$(U/U_m)_L$
0.0	0.0
1.0	0.33
2.0	0.63
3.0	0.85
4.0	0.96
5.0	1.00

Using Equations 41 through 44, the results for Test 9 are cited. In measuring impact pressure near a wall, the effective center of the probe is displaced away from the surface because of the local transverse velocity gradient. Young and Mass have found experimentally, for a flat-edged probe[20], that

$$\frac{\Delta y}{d_o} = 0.131 + 0.0083 \frac{di}{d_o} , \qquad (45)$$

where Δy is the upward displacement, and d_o and d_i are the outer and inner diameters of the probe. For Test 15,

$$d_o = 0.022 \text{ in.} = 0.00183 \text{ ft.}$$

$$d_i = 0.011 \text{ in.} = 0.000915 \text{ ft.}$$

This gives $\Delta y = 0.000158$ ft and

$$y_{effective} = \frac{d_o}{2} + \Delta y = 0.001073 \text{ ft.}$$

Calculations were performed at three distances from the leading edge. The results are noted in Table 5.

TABLE 5. TRANSITION CONFIRMATION*, 164 FPS FEE. PER SECOND

Parameter	Distance, Feet 1/2	1-1/2	4
δ_L, feet	0.00345	0.0060	0.00978
δ_T, feet	0.0133	0.032	0.0704
η	1.70	1.00	0.60
$(U/U_m)_T$	0.706	0.623	0.57
$(U/U_m)_L$	0.55	0.33	0.20
$(U/U_m)_{actual}$	0.57	0.35	0.49

* Test 9.

It is seen that up to the transition point, the actual velocity ratio matches that for a laminar boundary layer quite closely. The boundary layer up to 1.5 feet is clearly not turbulent according to the calculations. At 4 feet from the leading edge, the boundary layer is far from laminar (0.49 versus 0.2) showing that transition has occurred. On the basis of this analytical correlation, the experimental technique for detecting transition was confirmed and tests involving the corona apparatus were initiated.

THE EFFECT OF ELECTRICAL PERTURBATIONS ON TRANSITION

In order to conduct the electrical disturbance tests, or corona tests, it was necessary to select a flow speed and an associated disturbance with which to excite the boundary layer. At this time, it was decided to perform all subsequent tests at a flow speed of 175 fps. A test was run at 175 fps and transition was detected at 1.33 feet. With this determined, a transition Reynolds Number was estimated as follows:

Barometric Pressure, 29.5-in. hg

Temperature, 30°F

Flow Speed, 175 fps

Transition Distance, 1.33 feet

$$Re_{xtr} = \frac{\rho U_m x}{\mu} = \frac{0.078 \times 175 \times 1.33}{1.163 \times 10^{-5}} = 1.56 \times 10^6.$$

This corresponds to $Re_{\delta^*_{tr}} = 2140$.

The electrical disturbance was chosen to match the frequency and wavelength of the predominant boundary-layer oscillation at this Reynolds Number and would be applied to the flow in the pre-transition region. As discussed above, the precise location of the predominant oscillation is not known. However, it is known that the locus of predominant oscillations lies close to Branch II of the neutral stability curve within the amplified region. A point was chosen for a value of $\alpha\,\delta^* = \frac{2\pi}{\lambda}\,\delta^* = 0.24$. Using Equation 27,

$$\delta^* = 1.72\left(\frac{1.33\ 1.163 \times 10^{-5}}{175 \times 0.078}\right)^{1/2} = 0.00183 \text{ feet.}$$

This gives $\lambda = 0.048$ feet and $\lambda/\delta^* = 26.6$. The point is shown on Figure 5. To determine the frequency associated with the wavelength chosen, Figure 33 was constructed from information presented by Schubauer, Reference 5. It is seen from the figure that $\beta_r\,\nu/U_m^2 = 37.4 \times 10^{-6}$ at $Re_{\delta^*} = 2140$. Thus, the excitation frequency is $\beta_r/2\pi$, or

$$f = \frac{37.4 \times 10^{-6}\ U_m^2}{2\pi\,\nu} = \frac{37.4 \times 10^{-6} \times 175^2 \times 0.078}{2\pi \times 1.163 \times 10^{-5}} = 1215 \text{ cps.}$$

To completely characterize the oscillation, the wave speed is computed.

$$c_r = f\,\lambda = 1215\ (0.048) = 58.4 \text{ fps,}$$

and

$$c_r/U_m = 0.334.$$

The selected disturbance is shown as a point on Figures 4, 5, and 6 at $Re = Re_{xtr}$; the maximum total amplification associated with a wave of the above frequency is approximately 1000.

In order to isolate electrical effects, it was first necessary to conduct several "control" tests. The screw-studded plexiglass strips were installed beneath the plate and a test was conducted at 175 fps. The location of transition was unaltered, 1.33 feet. This is shown in Figure 34. Next the effects of wires suspended above the boundary layer were determined. Two possible mechanisms which could trigger a premature transition were present, boundary-layer entrainment by the wake behind the wires, and physical vibration of the wires. Twenty-two wires were installed, at a longitudinal spacing of 0.048 feet, covering the region from 0.917 to 1.940 feet from the leading edge. The wires were 0.004 inch in diameter. Each wire was spaced 9/16 of an inch from the surface of the plate to allow clearance for the 1/2-inch-diameter portion of the pressure probe. This 9/16-inch distance was held for all tests involving corona wires. Several tests were conducted at 175 fps with the wires installed. Transition was located consistently at 0.834 feet from the leading edge. This was immediately in front of the first wire. It is believed that some distance downstream from the normal transition point, the rapidly thickening boundary layer and the wake left by the wires intermixed, entraining the boundary layer to the plane of the wires. This entrainment propagated upstream until the first wire was reached. To demonstrate that the premature transition was, in fact, caused by the downstream wires, one 0.008-inch wire was suspended at a distance of

1.3 feet from the leading edge. Transition occurred downstream of the wire at 1.417 feet from the leading edge. The data from the above tests are also shown on Figure 34. Additional evidence is presented with the descriptions of the corona tests substantiating the fact that a series of wires may be suspended, above the boundary layer, in the pretransition region without tripping transition.

The corona tests were initiated by suspending three wires, 0.008 inch in diameter, at distances of 1.209, 1.258, and 1.307 feet from the leading edge. A test was conducted at zero current for which normal transition was expected at 1.33 feet. Instead, the transition occurred at 0.83 feet. This corresponds to a free stream turbulence intensity of about 0.4 percent. The corona was turned on leaving the premature transition unexplained for the moment.

Two observations can be made from the test results shown on Figure 35:

(1) The location of transition was unaffected by the corona discharge, both with and without the controlled frequency component (1215 cps).

(2) A decrease in impact pressure behind the last wire was present when the discharge was on, both with and without the controlled frequency component.

In an effort to determine the cause of the premature transition, the wires were removed and the flow adjustment doors set fully open to lower the flow speed. If the transition point were now

located downstream of 1.33 feet, the premature transition could be attributed to presence of the wires. If, however, the transition point was between 0.83 feet and 1.33 feet, the wires were probably not the cause. A test was conducted at 153 fps and transition was located at 1.17 feet. Three wires were immediately installed, at distances of 1.063, 1.112, and 1.16 feet from the leading edge, and a test was conducted at 153 fps with and without current. Provision was not made to change the wire spacing but the excitation frequency was increased to compensate for the change in location on the stability diagram, Figure 4. These observations may be made from the test results shown in Figure 36:

(1) Transition was not tripped by the wire.

(2) The location of transition was unaffected by the corona discharge, both with and without the controlled frequency component.

(3) The impact pressure dip marking transition was accentuated in the presence of the discharge, both with and without the controlled frequency component.

At the conclusion of this series of tests, the reason explaining the premature transition at 175 fps was made evident. A guard rail had been recently installed just outside the entrance to the tunnel. The rail may be seen in Figure 16. The obvious effect of the rail was to increase the free stream turbulence. This caused the normal transition to move from 1.33 feet to 0.83 feet. The rail was removed for the final series of tests now to be described.

Following the experimental procedure outlined above, a final series of corona tests was conducted at 174 fps. The first test was performed with no wires installed. The static pressure distribution for this test is shown in Figure 26. Transition was located at 1.25 feet. Four wires (0.008-inch diameter) were then installed from 1.063 to 1.209 feet from the leading edge at a spacing of 0.048 feet. Another test was conducted at 174 fps with no current on. The transition was essentially unchanged, 1.27 feet. For the next part of the test, the electrical disturbance was activated. The corona parameters were as follows:

Current, 1 ma

Voltage, 9 kvdc plus 2 kvac peak-to-peak

Frequency, 1215 cps.

The transition point shifted downstream to 1.42 feet. At 1.27 feet, the pressure readings were now steady and transition was not apparent.

To confirm the transition shift, the current was later turned completely off. Impact pressure readings were taken immediately at 1.42 feet and 1.27 feet. Fluctuating pressure readings at a given distance from the leading edge signify the presence of transition, as discussed above under DETECTING TRANSITION. Once again, the pressure readings were steady at 1.42 feet and fluctuating at 1.27 feet, indicating that the transition had jumped back upstream. The data for the tests just described are presented in Figure 37. Leading edge data have been omitted to preserve scale. All sets of data terminate at 33.2 feet of water at the leading edge.

During the test, three sweeps of excitation frequency were made. The sweeps were made at probe positions of 2 feet, 1.42 feet, and 1 foot from the leading edge. At each frequency, shown on Figure 38, one-half minute was waited before recording the impact pressure. Shifting between readout frequencies was accomplished by slowly adjusting the oscillator with the vernier knob. In this manner, it was felt that any resonant or unusual effects would be revealed. Such was not the case, for the transition apparently remained at 1.42 feet regardless of the frequency. This was also true for zero frequency, or straight d-c corona.

DISCUSSION OF RESULTS

The effect of electrical disturbance on transition will be discussed. In the preceding section, it was demonstrated that corona discharge may be used to forestall transition under certain conditions. Several questions arise regarding the phenomenon. What is the mechanism by which transition was forestalled? Why was the transition insensitive to the electrical disturbance frequency? Lastly, why was the transition affected at the flow speed of 175 fps and unaffected at 153 fps?

In an effort to disclose the mechanism influencing transition, several characteristics of the electrical discharge will be brought forth. First, for a constant sustained discharge, the total velocity of the ions is the sum of air velocity and the velocity of the ions in the air.

$$\bar{v}_t = \bar{v}_{ion} + \bar{v}_a \,. \tag{46}$$

The velocity of the ions in air is given by the product of the field strength and the ion mobility

$$\bar{v}_{ion} = K \bar{E} \,. \tag{47}$$

For a positive wire corona, it may be assumed that only positive ions exist in the major portion of the wire-to-plate gap. For air at normal pressure and temperature, Reference 16 gives a value of 0.00146 ft^2/volt-sec for the mobility of singly charged positive ions. If the field between the parallel wires and the plate is approximated as that

between two parallel plates, the field voltage drop may be taken as half the wire-to-plate voltage because of the sharp voltage peak near the wires. Therefore, the field strength is approximated by

$$\bar{E} = \frac{(10{,}000/2) \text{ volts} \times 12 \text{ in.}}{9/16 \text{ in.} \quad \text{ft}} = 107{,}000 \text{ volts/ft} . \qquad (48)$$

Using Equation 47 gives an ion velocity of 156 fps.

The ion velocity is close to the air flow velocity outside the boundary layer. The ions are, therefore, impinging on the boundary layer at approximately a 45-degree angle. The relative absolute velocity of the neutral air molecules in the corona wind will be about 5 fps[21]. Thus, the neutral air molecules impinge on the boundary layer at a shallow angle. The static pressure increase at the plate that would be associated with a direct corona wind, that is if the tunnel flow velocity were zero, is of the order of only 0.001 feet of water, according to actual experiments performed in Reference 12. However, it demonstrated that such a corona wind is capable of greatly depressing a convective boundary layer with associated drastic increases in local heat-transfer coefficient. It is postulated that similar boundary-layer depression is occurring in the present experiment to a lesser extent. In the absence of a boundary-layer mouse, this could not be verified.

The boundary-layer depression manifests itself by causing high velocity streamlines to be brought closer to the surface of the plate in the region adjacent to, and downstream of, the wires. This may be seen in Figure 36 independent of transitional effects.

Hypothetically, if the wires are positioned immediately upstream from the transition point, boundary-layer depression would imply two things. First, the boundary layer is being physically confined to the plate. Second, the thinning boundary layer will have associated with it a local negative static pressure gradient in the flow direction. It is well known that transition is retarded by a favorable pressure gradient. Thus, boundary-layer depression may be the mechanism explaining the effect of the electrical disturbance on transition.

The lack of response to the controlled frequency component of the electrical disturbance may be explained in several ways. It is felt that one of the primary reasons is insufficient intensity of the a-c component. Current contributions associated with the pulsating disturbance were an average of 20 μa. This is 2 percent of the total corona current. Another reason may be improper matching and phasing of the disturbance with local predominant boundary-layer oscillation. Hot-wire equipment would be required to determine the actual wave properties of laminar boundary-layer oscillations present in the flow. Without this, choosing a disturbance from the theoretical neutral stability curve could never precisely match a predominant oscillation. Furthermore, it is not known by what mechanisms the amplification process would be disrupted even if proper matching and phasing could be accomplished. However, it can be concluded from the experiment that the controlled frequency component of the disturbance did not have a detrimental effect on the amplification process. This would cause premature transition.

In Test 17, transition was forestalled by the action of the corona while in Test 15 it was not. In both tests, the corona wires were positioned immediately upstream of the normal transition location. The explanation lies in the difference of free stream turbulence intensity between the two series of tests. Recall that Tests 14 and 15 were conducted in the presence of the outside guard rail while Test 17 was not. As mentioned above, the deduced free stream turbulence intensity associated with Test 15 was 0.4 percent and that for all other tests was approximately 0.3. This 30 percent increase in background turbulence might well be the swaying factor in determining whether or not the corona discharge is capable of influencing transition. From this it may be suggested that future investigations be conducted at the lowest possible levels of free stream turbulence.

SUMMARY OF CONCLUSIONS AND RECOMMENDATIONS

The conclusions resultant from this experimental investigation are summarized below in chronological order.

(1) To assure proper development of a laminar boundary layer, on a flat plate with an asymmetric sharp nose, requires the use of flow "blockage" techniques on the active side of the plate.

(2) A near-surface impact probe has proved to be a reliable and convenient tool for detecting boundary-layer transition providing the probe tip size is carefully chosen. It was found that a tip diameter approximately equal to 1/3 the laminar boundary-layer thickness at transition (δ_{tr}) was quite satisfactory from the aspects of both response and sensitivity.

(3) It was found that rows of wires oriented at right angles to the flow; suspended at a distance of $9 \times \delta_{tr}$ from the flow surface and extending from the normally laminar region deep into the turbulent region, cause transition to occur at the wire farthest upstream. Wires similarly suspended in only the pre-transition region do not trip transition.

(4) Transition is sensitive to free stream turbulence. Small flow obstructions outside the intake zone of the wind tunnel may cause premature transition.

(5) Under conditions of low free stream turbulence, a steady corona discharge applied to the boundary layer in the pre-transition region can forestall transition. Boundary-layer depression is the

likely mechanism involved. This was accomplished at a mean flow speed of 175 fps.

(6) Superposition of a controlled frequency component on the steady corona discharge did not affect the result stated in (5), nor did it promote premature transition. A wide range of frequency was scanned. The failure of the controlled frequency excitation to interact with the selective boundary-layer amplification process is attributed to lack of intensity and precise matching of wave parameters.

In the light of the experimental findings, it appears logical to continue further investigation of electric effects on boundary-layer transitions. Some recommendations regarding the course and methods of such experimentation are presented.

(1) The free stream turbulence intensity should be low, certainly below 0.3 percent.

(2) A hot-wire anemometer should be employed to probe the boundary layer for thickness, laminar oscillations, and transition.

(3) In addition to detecting the natural disturbances present in the boundary layer, provision should be made to determine the effects of the forced perturbations. Local pressure changes caused by the action of the corona may be sensed with suitably placed, sensitive instrumentation.

(4) Means for attaining a controlled frequency disturbance of greater intensity should be sought.

(5) With respect to the present electrical configuration, provision to vary the wire spacing and positions would be most desirable. The effects of wires positioned near the leading edge and into the transition region should be explored.

(6) Different electrode configurations should be investigated.

(7) Slower flow speeds may be beneficial in highlighting sensitive ion-fluid interactions.

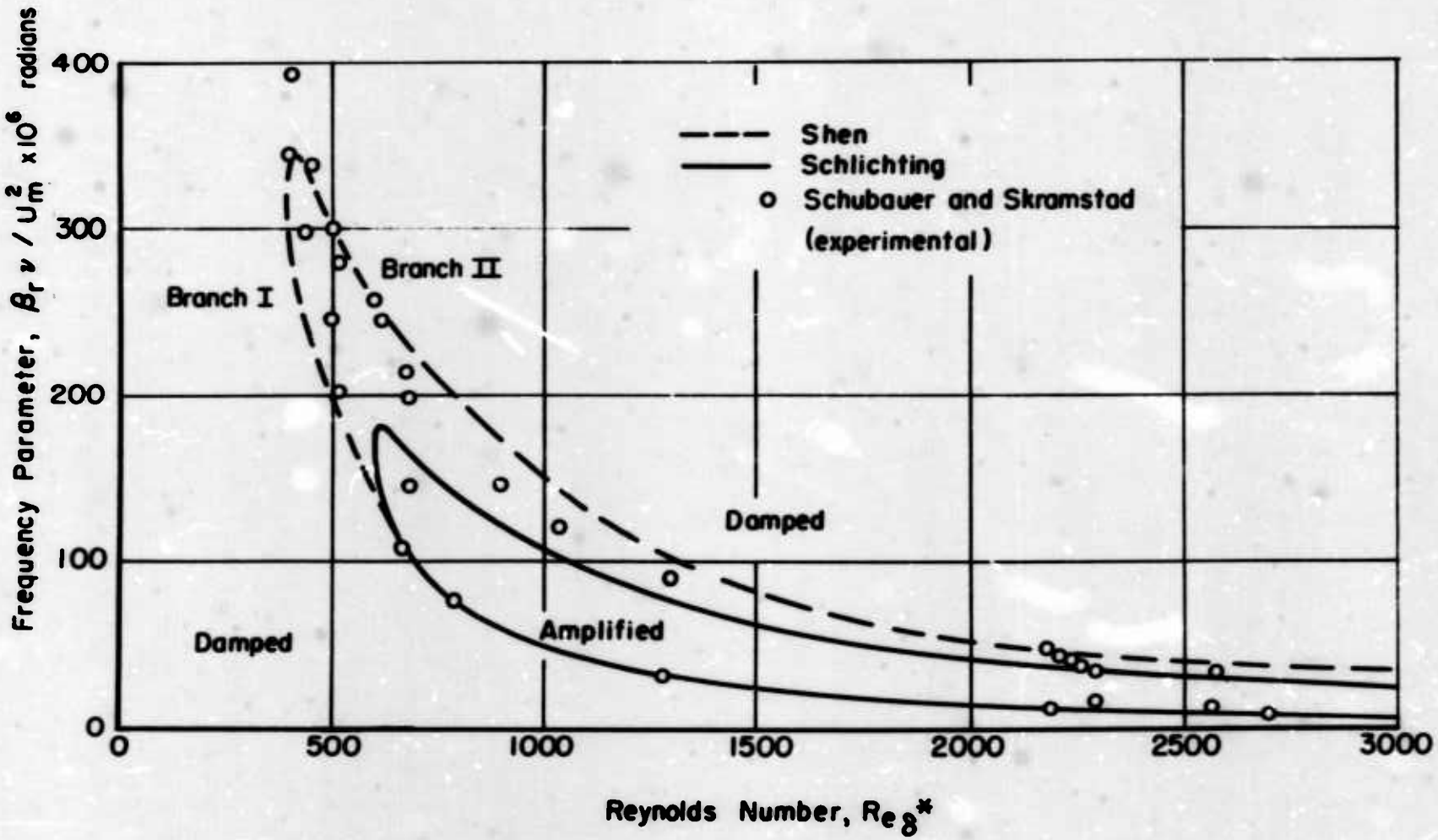

FIGURE 1. NEUTRAL STABILITY CURVE IN TERMS OF REYNOLDS NUMBER AND FREQUENCY PARAMETER

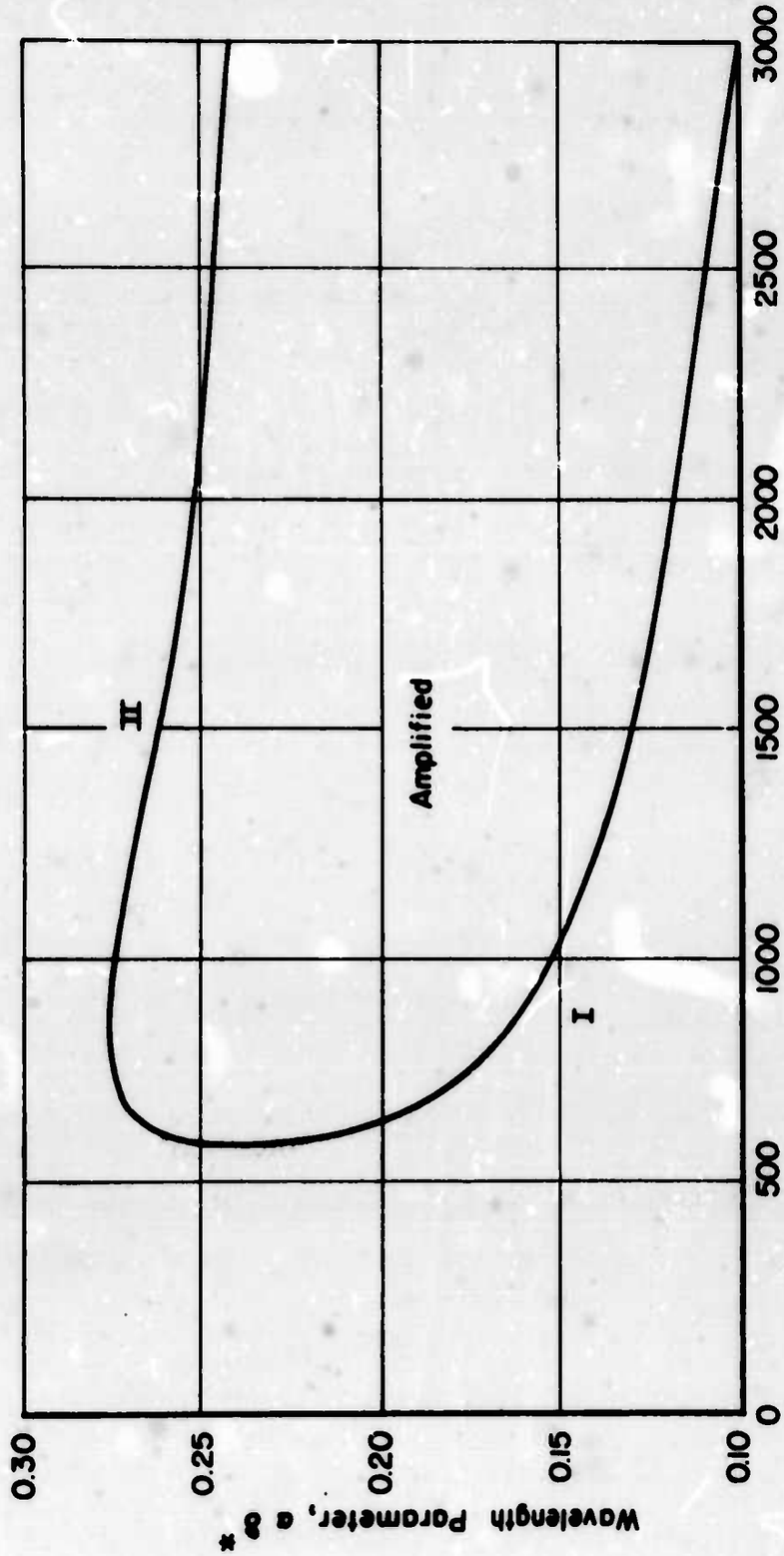

FIGURE 2. NEUTRAL STABILITY CURVE IN TERMS OF REYNOLDS NUMBER AND WAVELENGH PARAMETER

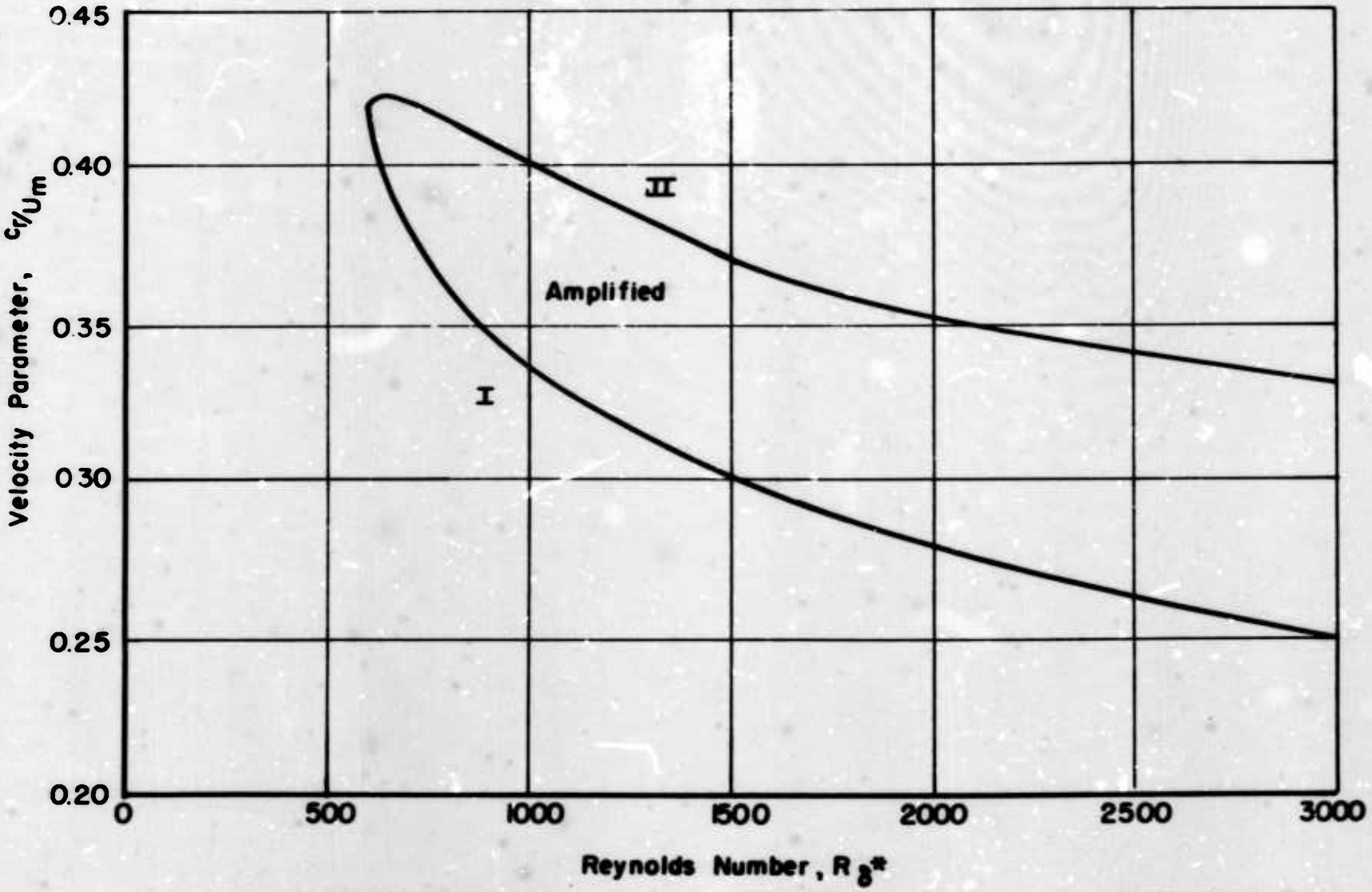

FIGURE 3. NEUTRAL STABILITY CURVE IN TERMS OF REYNOLDS NUMBER AND VELOCITY PARAMETER

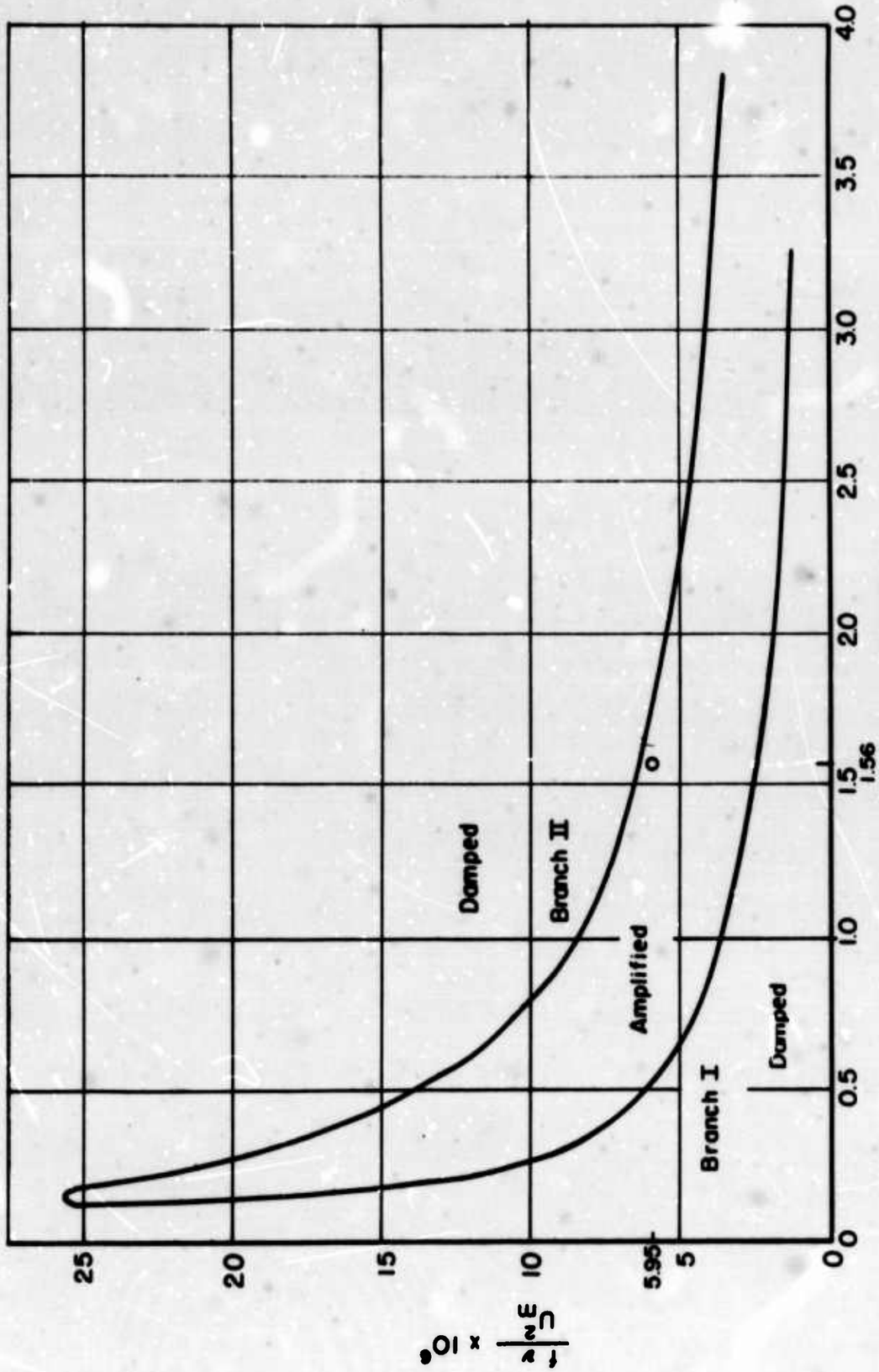

FIGURE 4. NEUTRAL STABILITY CURVE IN TERMS OF REYNOLDS NUMBER (Re_x) AND FREQUENCY

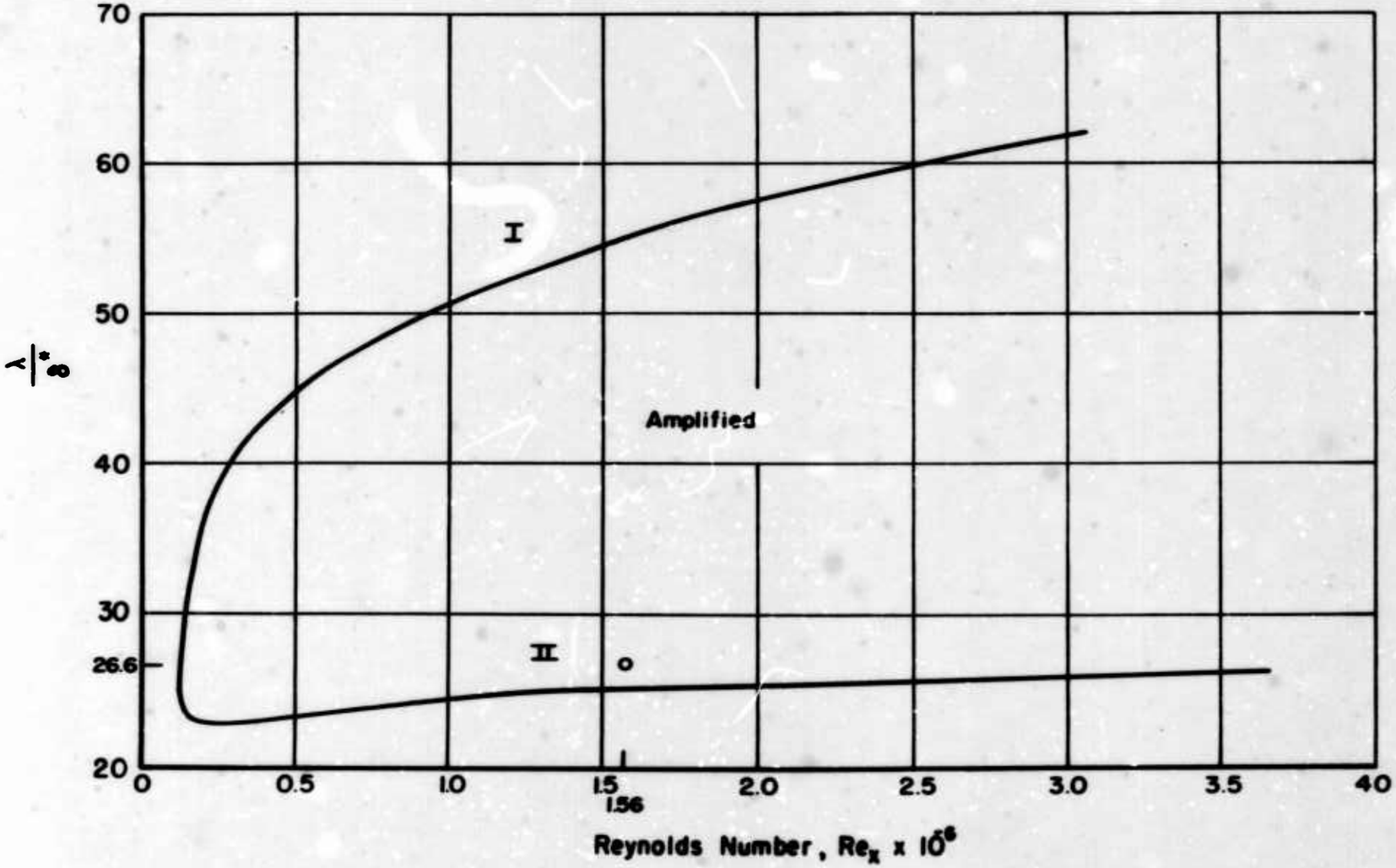

FIGURE 5. NEUTRAL STABILITY CURVE IN TERMS OF REYNOLDS NUMBER (Re_x) AND WAVELENGTH

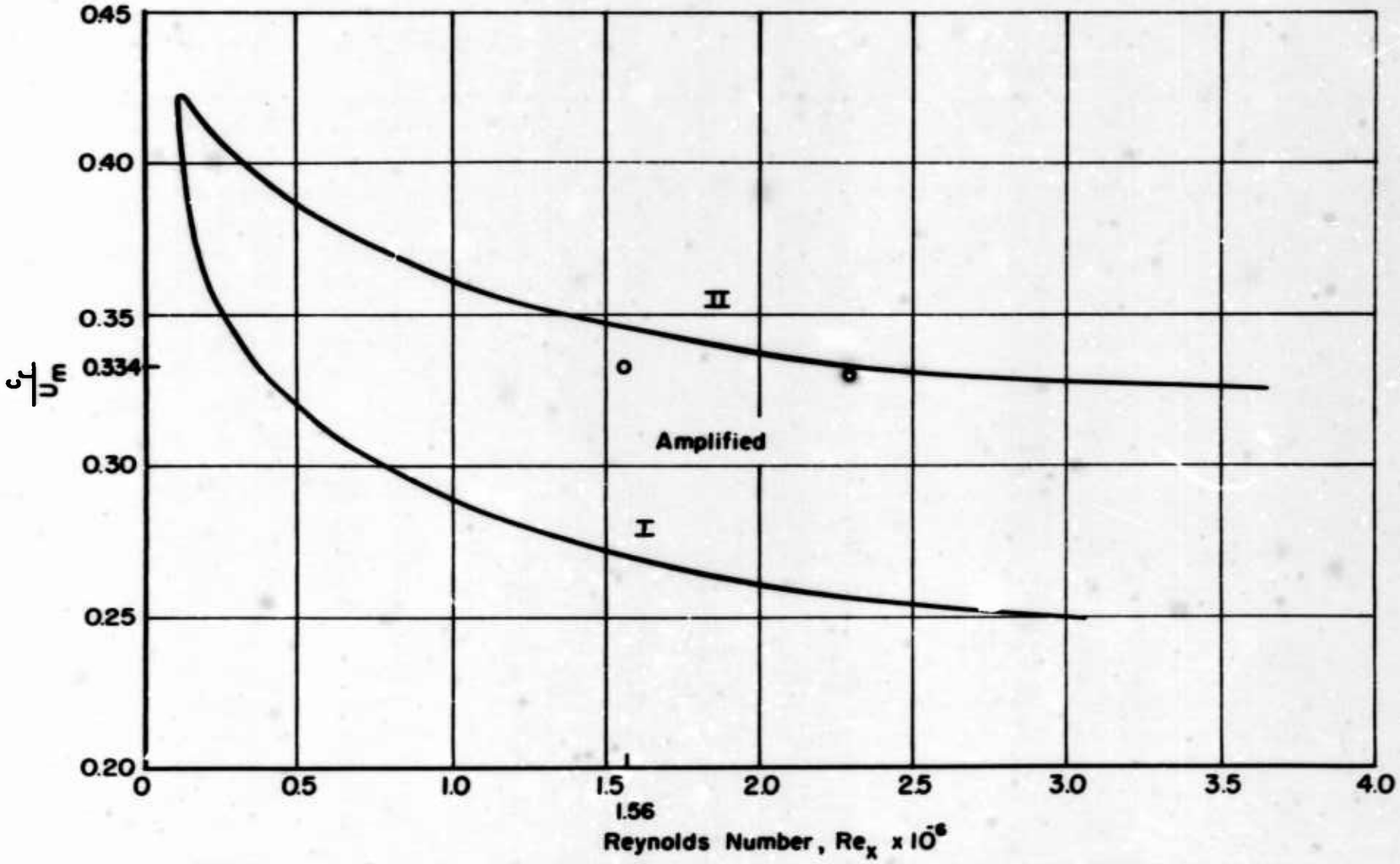

FIGURE 6. NEUTRAL STABILITY CURVE IN TERMS OF REYNOLDS NUMBER (Re_x) AND VELOCITY PARAMETER

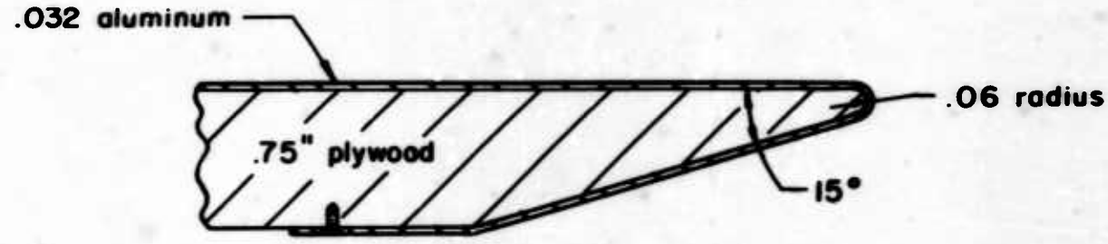

a. Rounded Nose

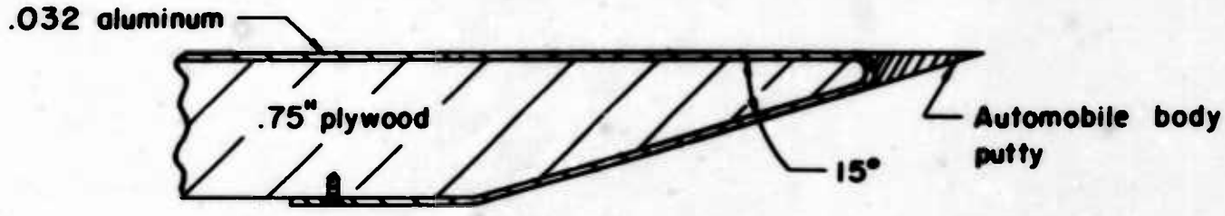

b. Sharp Nose

FIGURE 7. SECTION VIEW OF FLAT PLATE LEADING EDGES

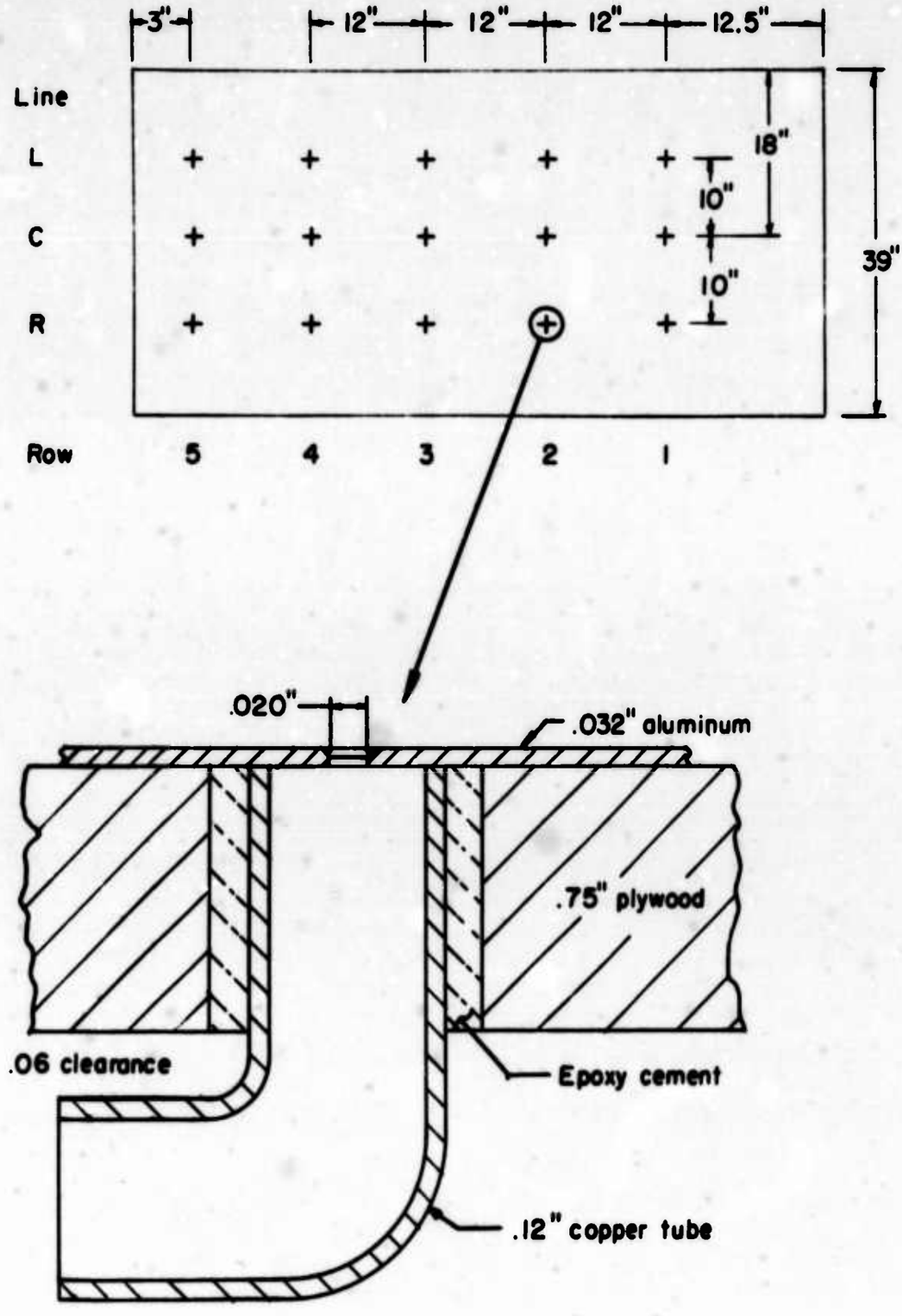

FIGURE 8. FLAT PLATE STATIC PRESSURE TAPS

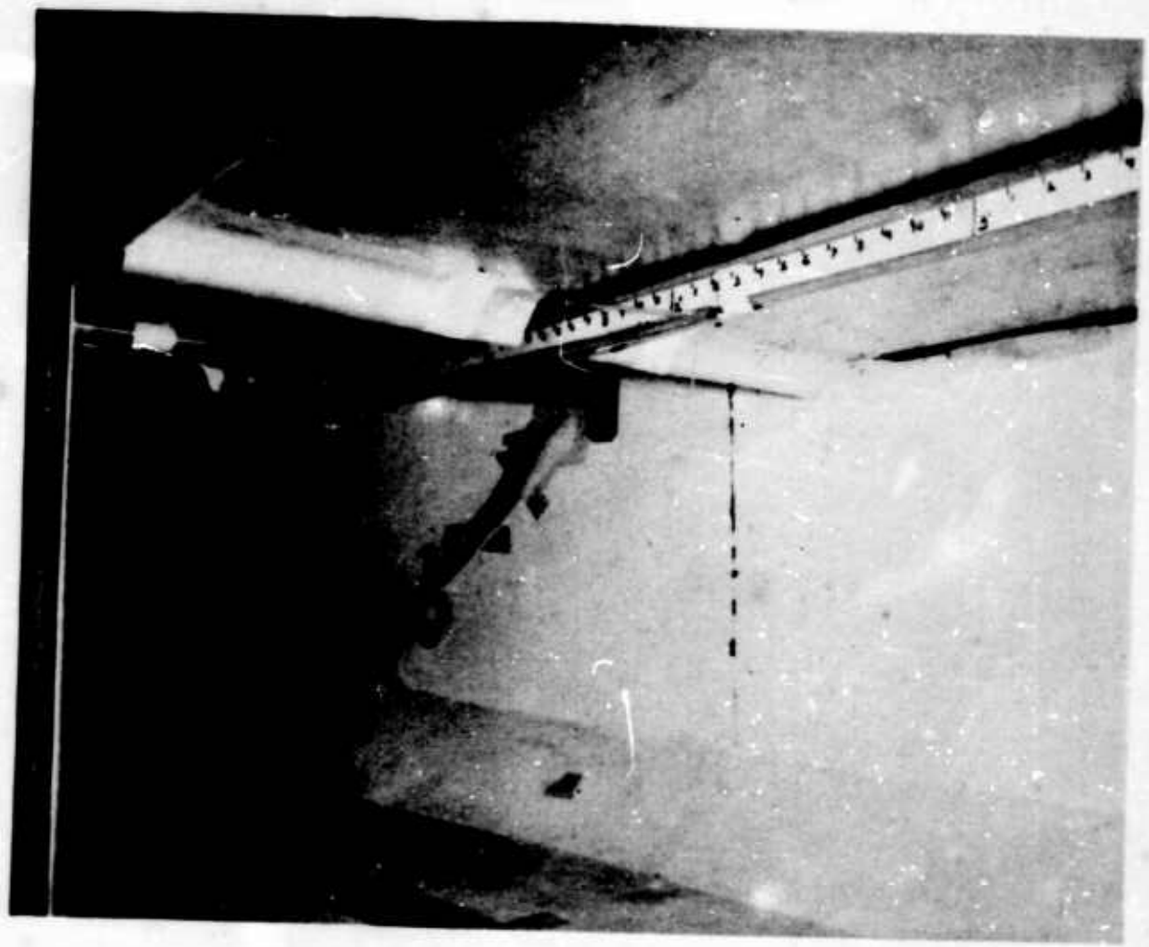

FIGURE 9. REARWARD VIEW OF ACTIVE SIDE OF PLATE

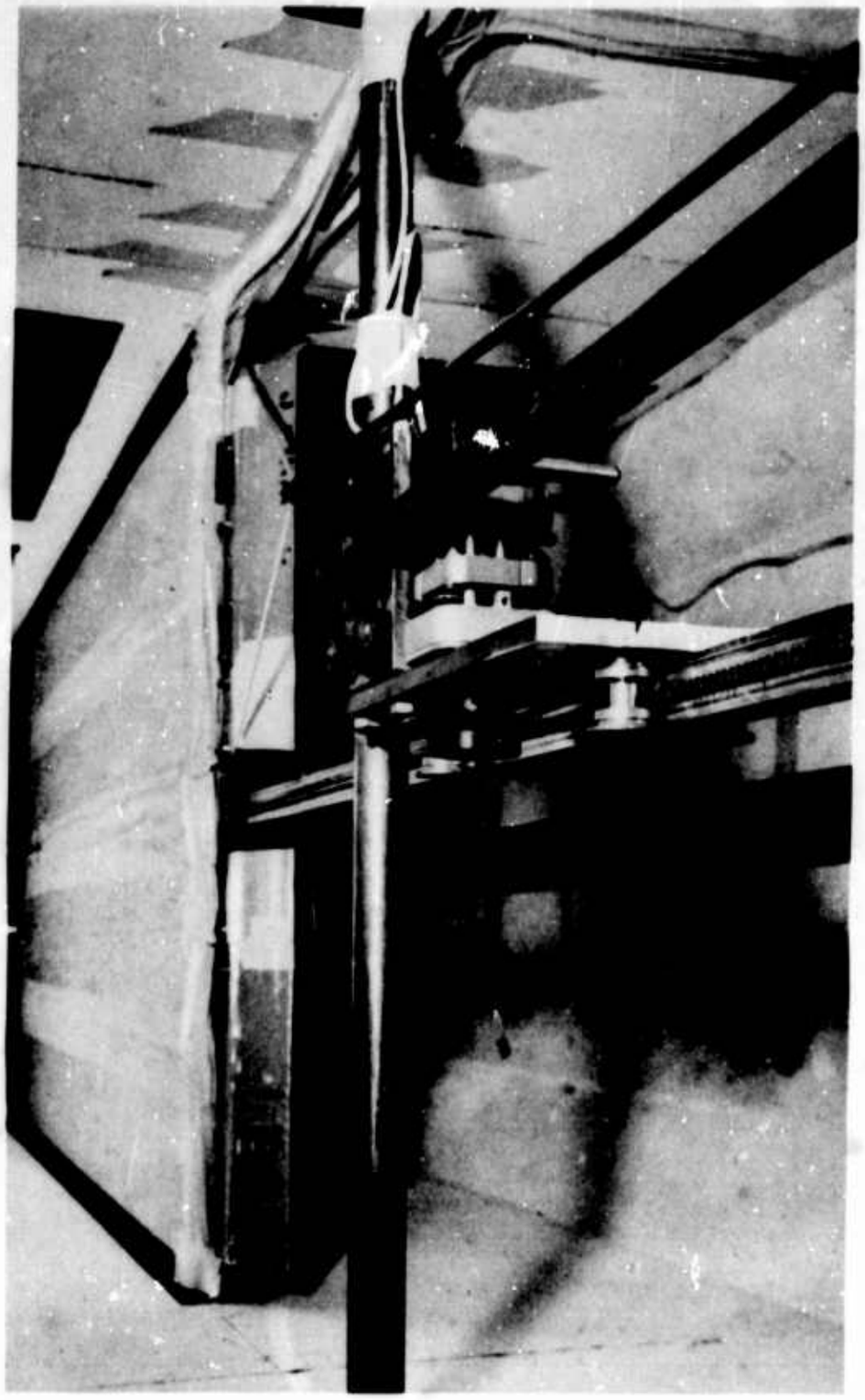

FIGURE 10. DOWNSTREAM VIEW OF TEST SECTION

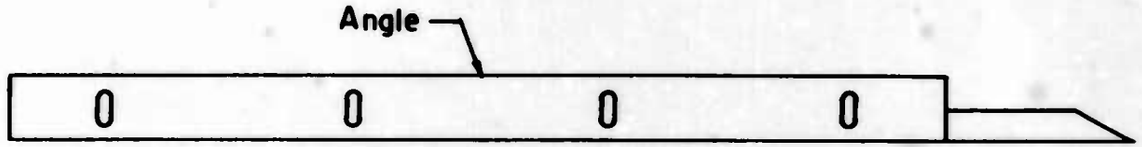

Side View

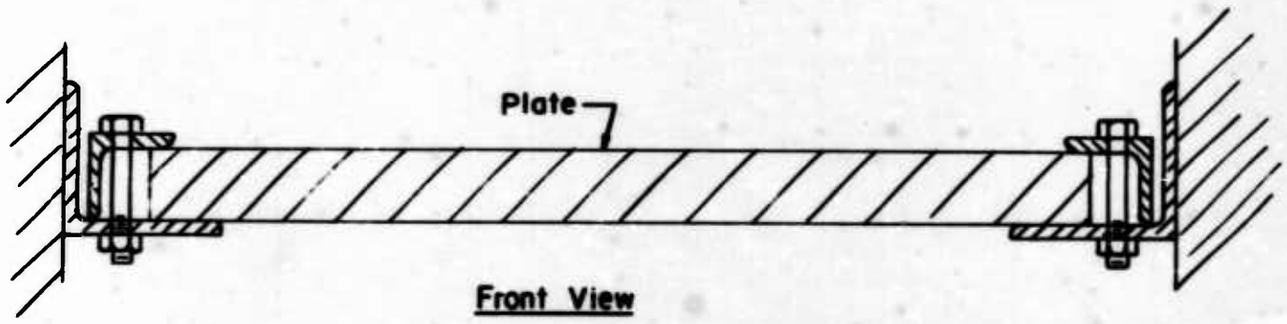

Front View

FIGURE 11. FLAT PLATE MOUNTING DETAIL

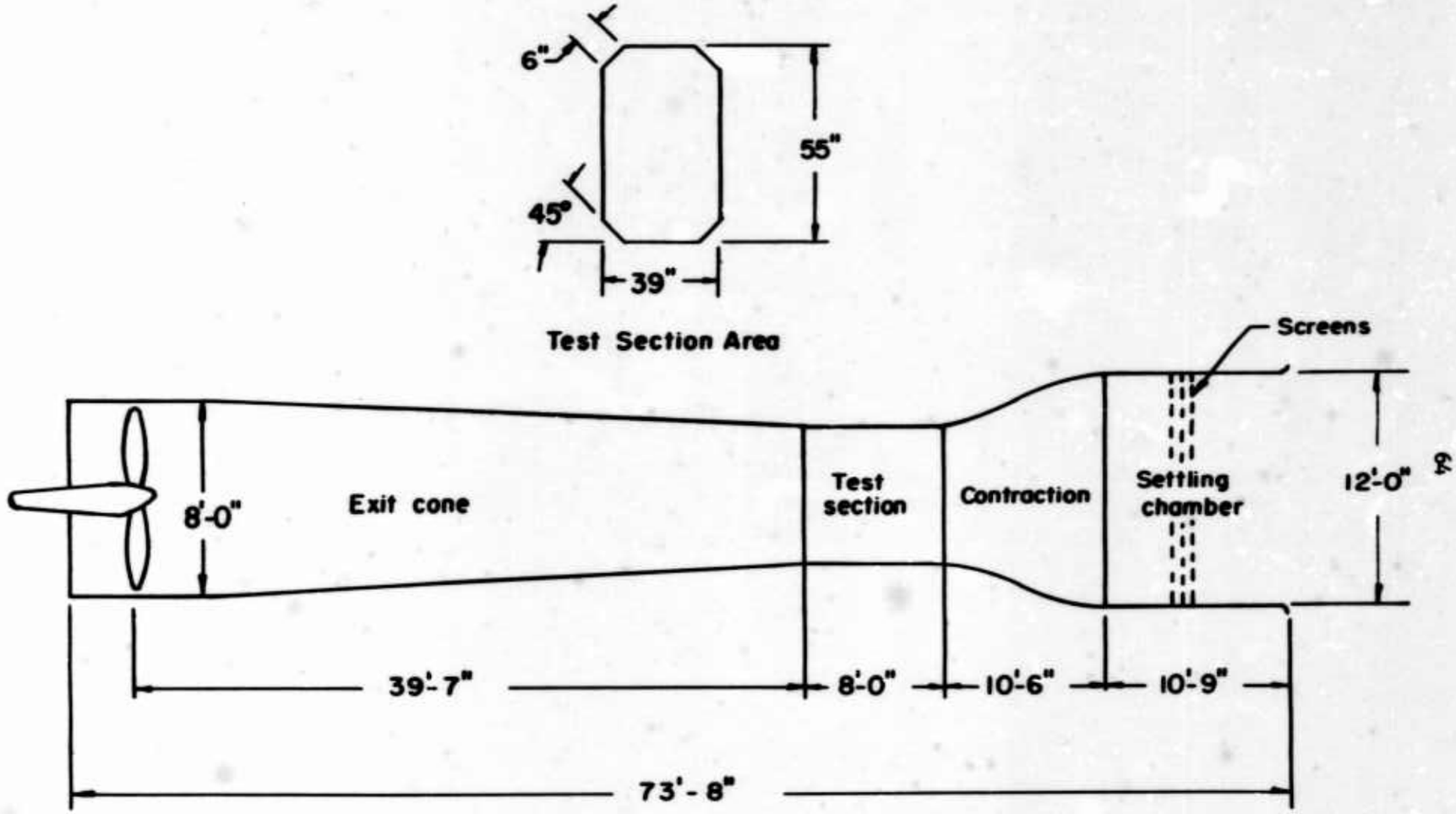

FIGURE 12. ELEVATION VIEW OF WIND TUNNEL

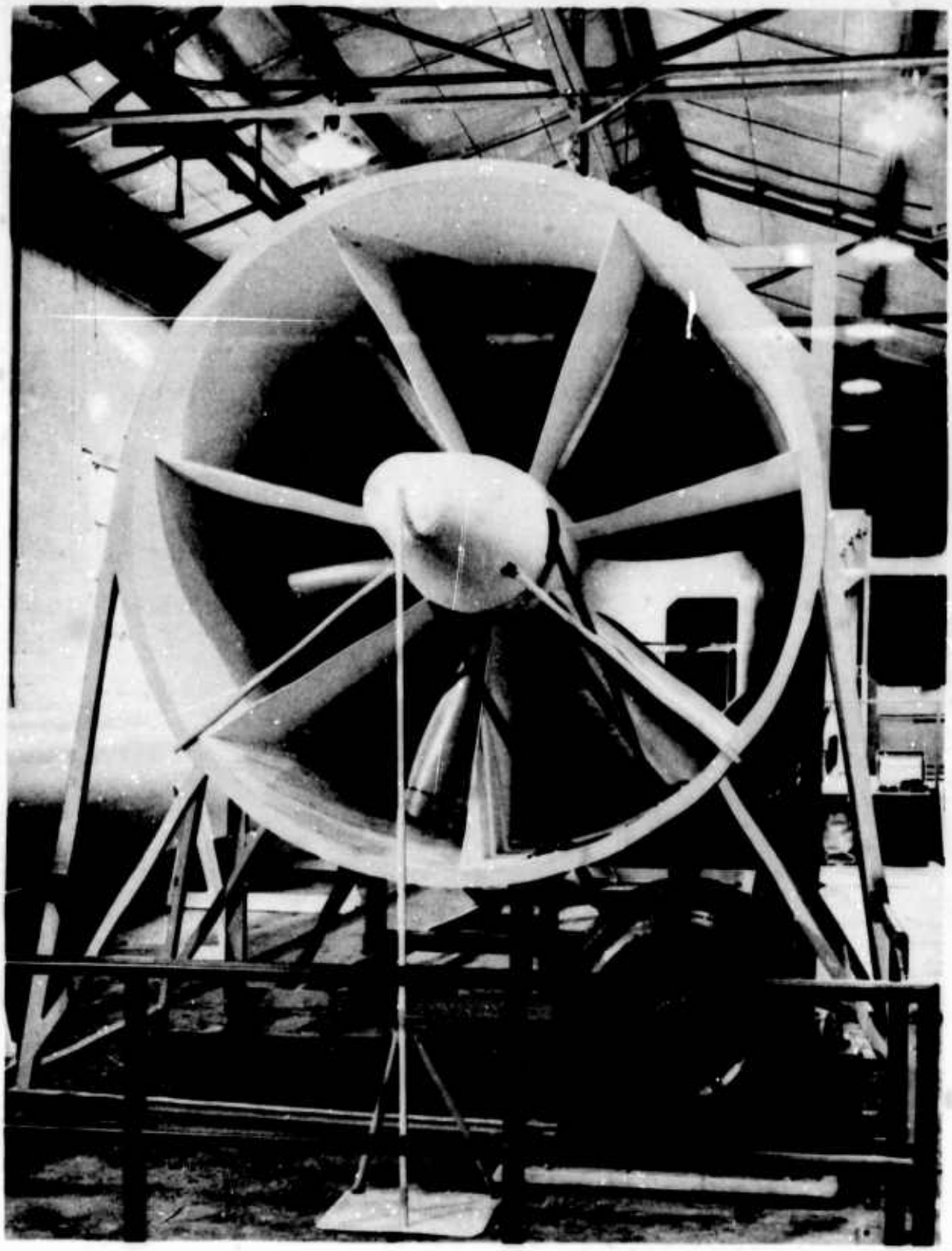

FIGURE 13. WIND TUNNEL EXHAUST FAN AND MOTOR

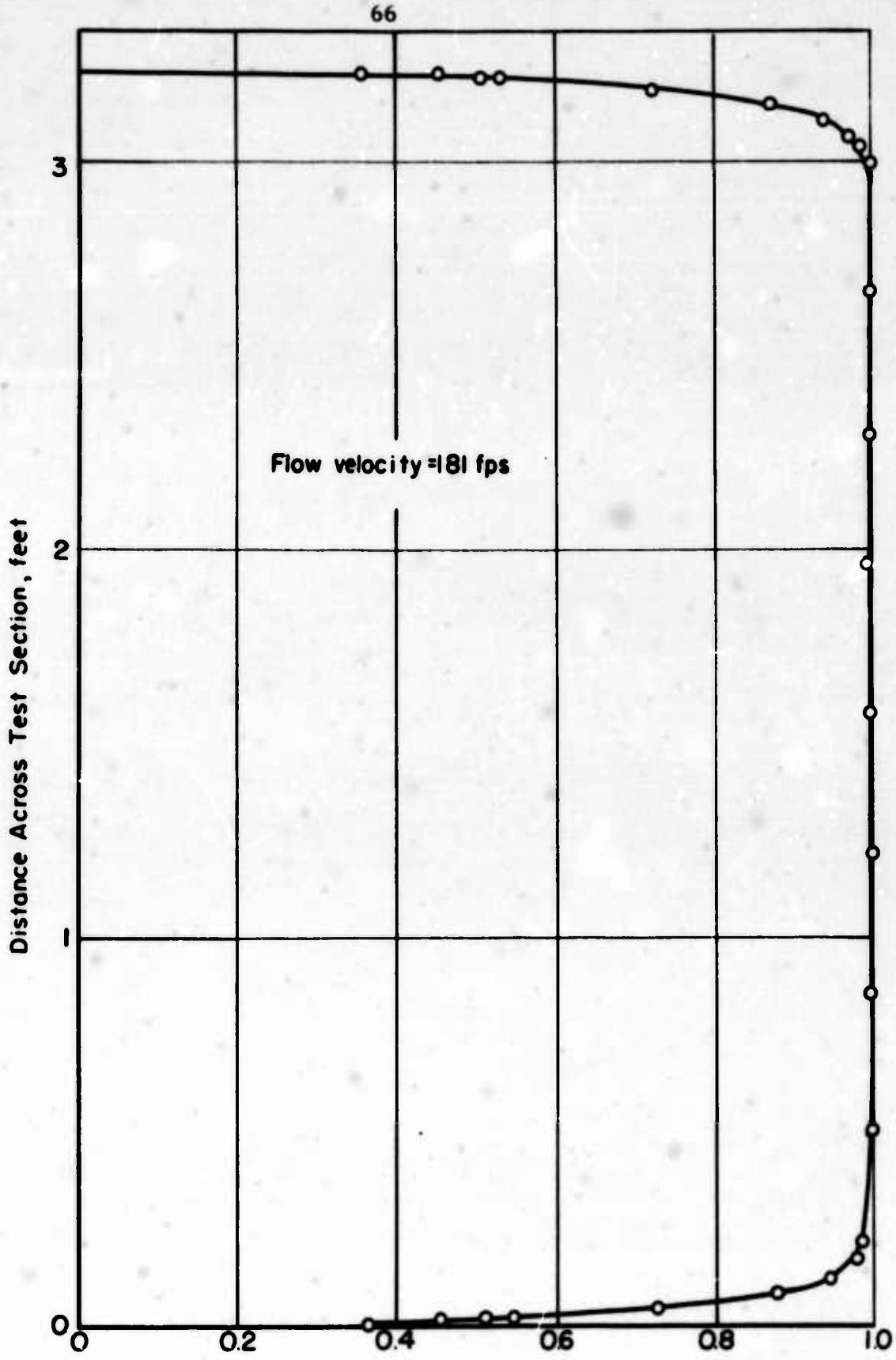

FIGURE 14. HORIZONTAL DISTRIBUTION OF DYNAMIC PRESSURE AT CENTERLINE OF TEST SECTION

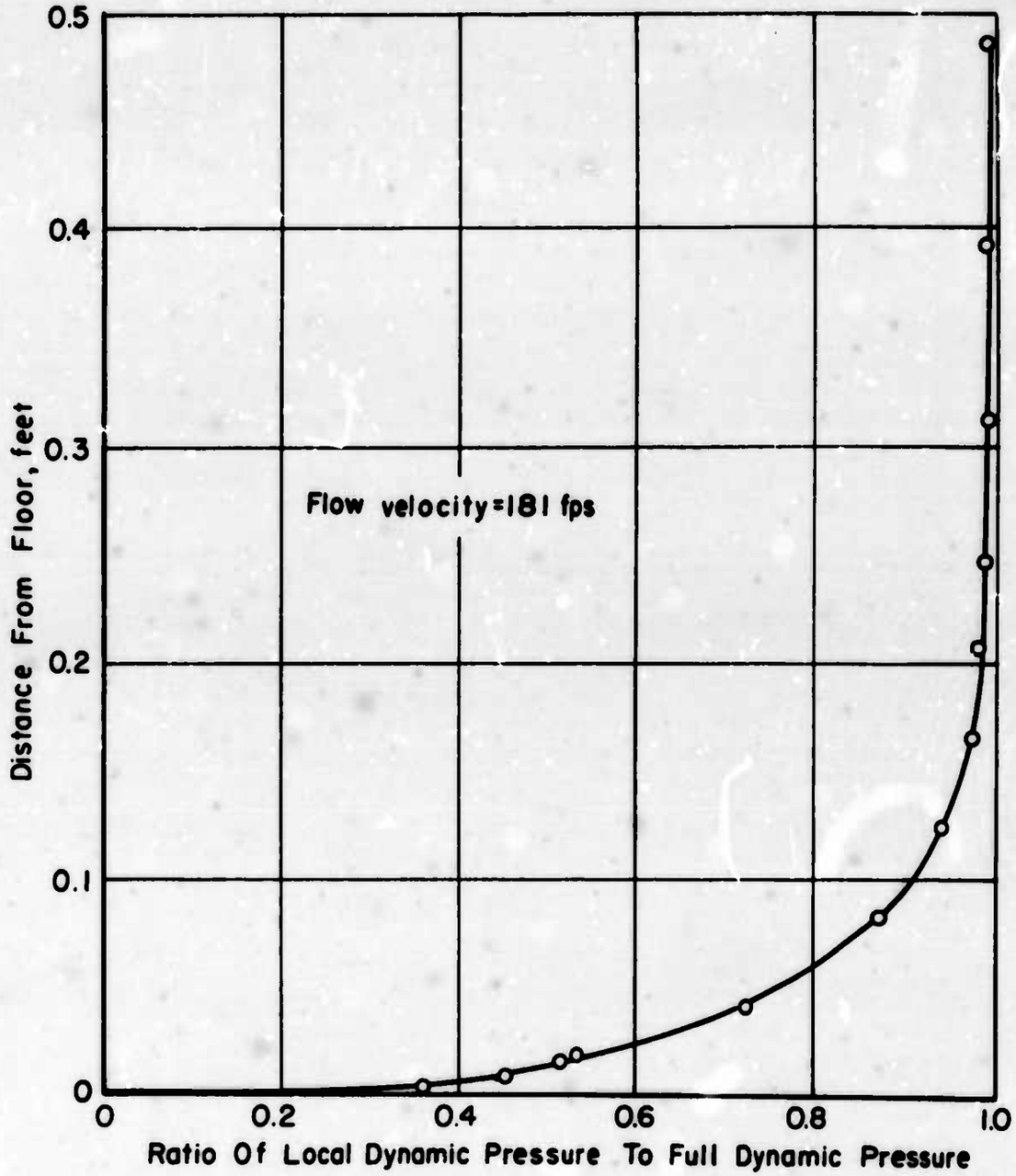

FIGURE 15. WALL BOUNDARY LAYER AT THE VERTICAL CENTERLINE OF WIND TUNNEL TEST SECTION

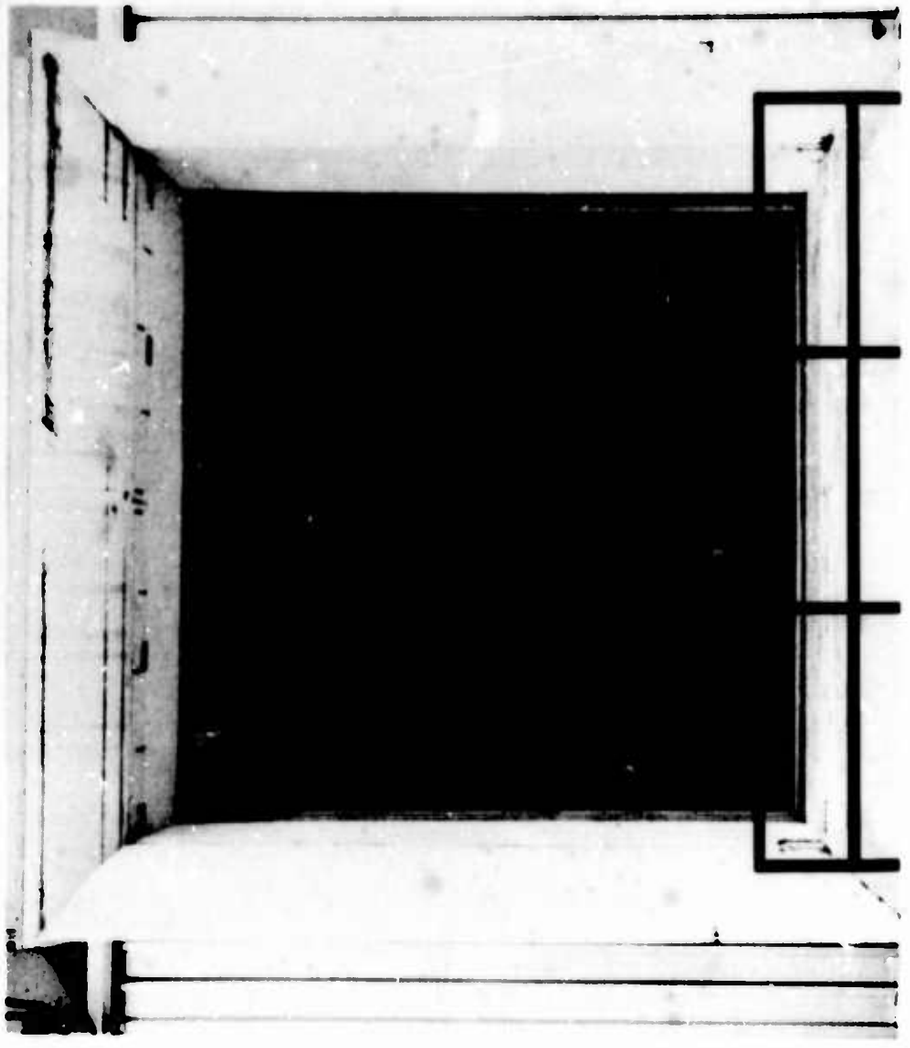

FIGURE 16. WIND TUNNEL AIR INTAKE AREA

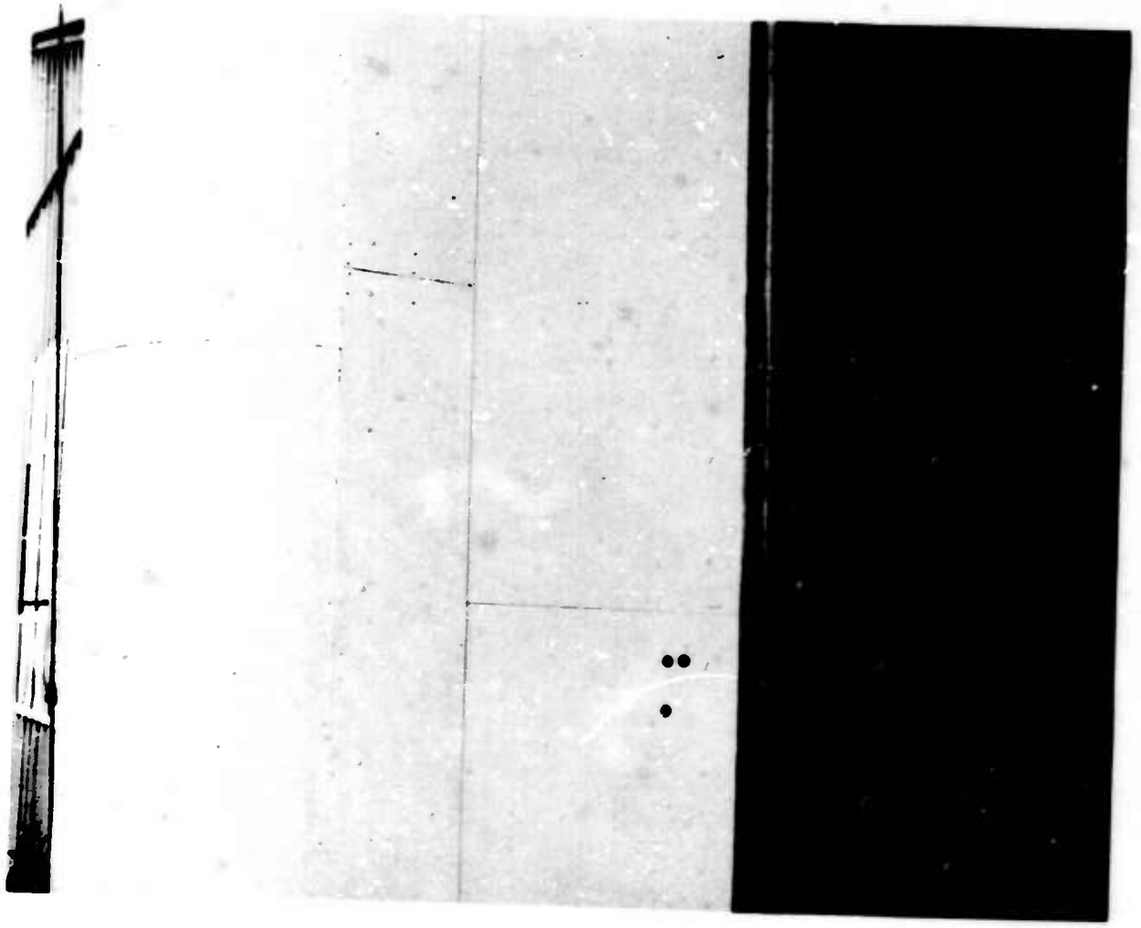

FIGURE 17. TURBULENCE SCREENS NEAR WIND TUNNEL AIR INTAKE AREA

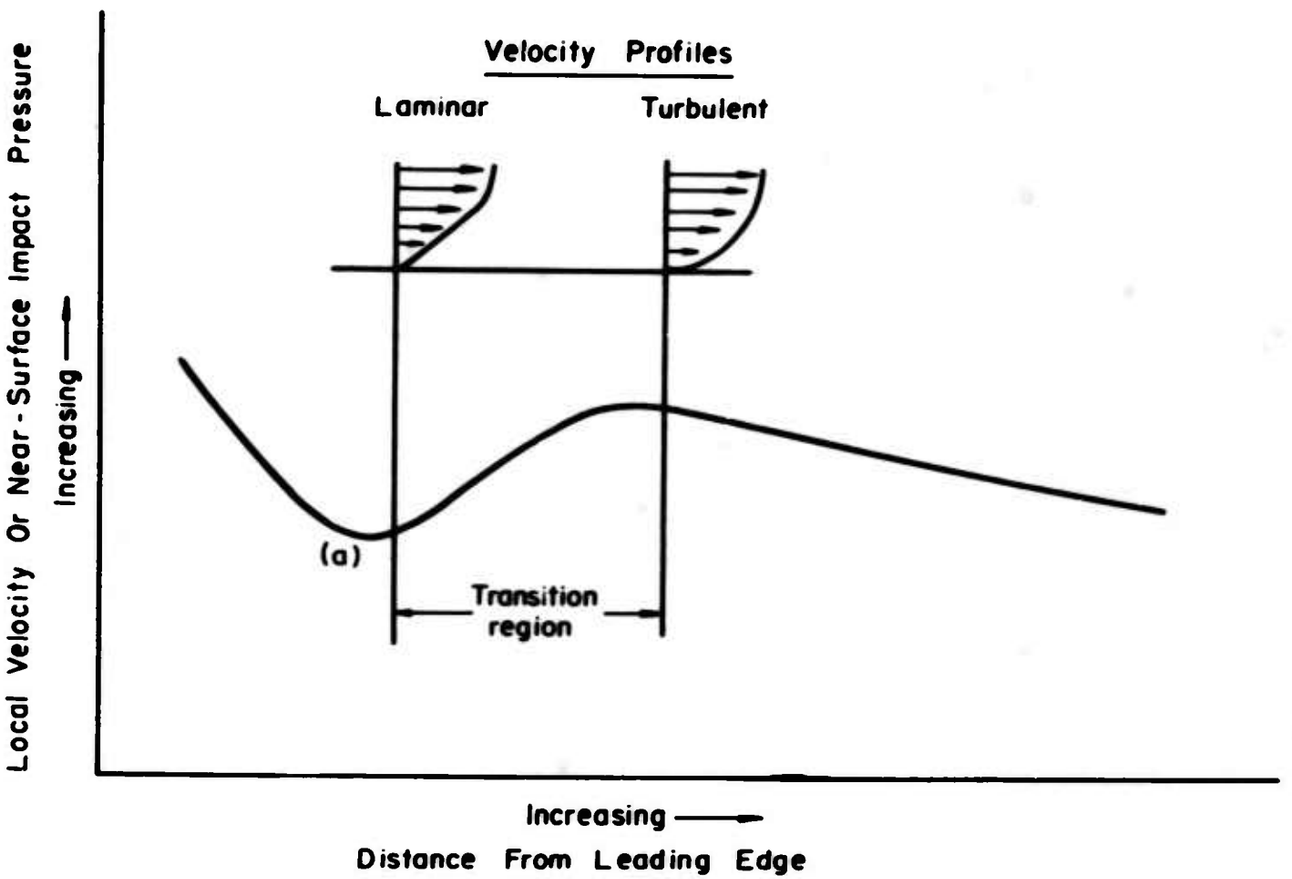

FIGURE 18. IMPACT PRESSURE IN THE BOUNDARY LAYER AT A SMALL CONSTANT HEIGHT ABOVE THE SURFACE

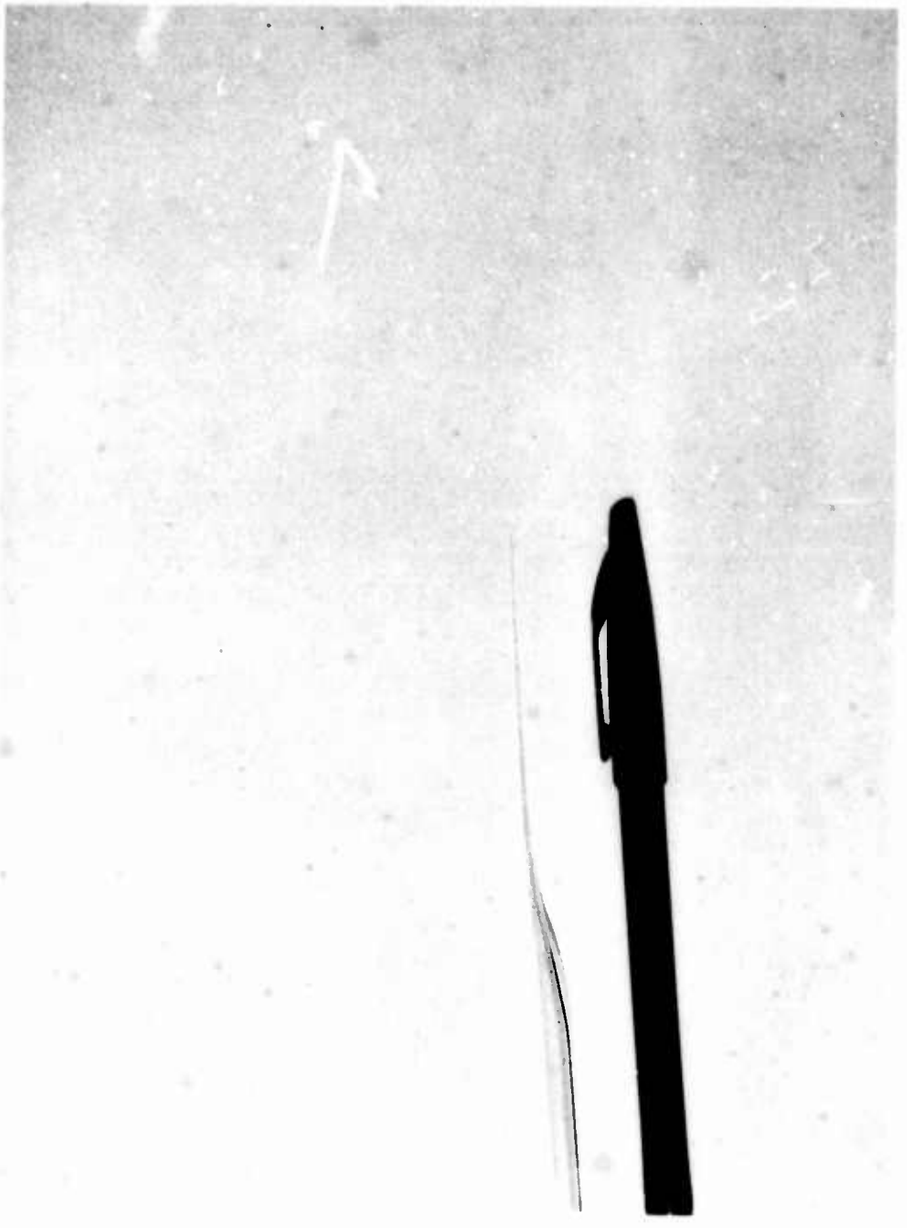

FIGURE 19. CLOSEUP OF A GLASS PRESSURE PROBE TIP

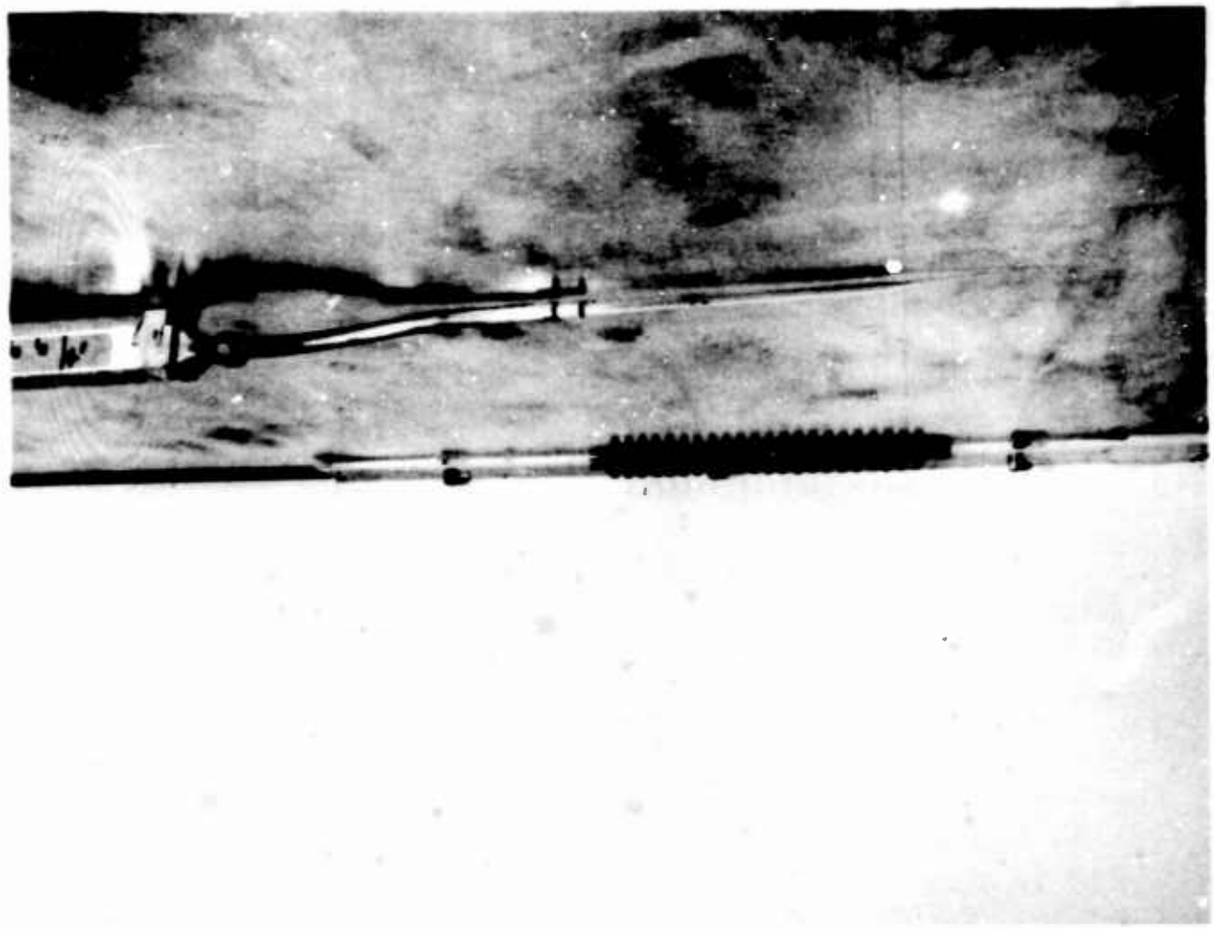

FIGURE 20. UNDERSIDE OF PLATE SHOWING PRESSURE PROBE ASSEMBLY AND CORONA WIRES

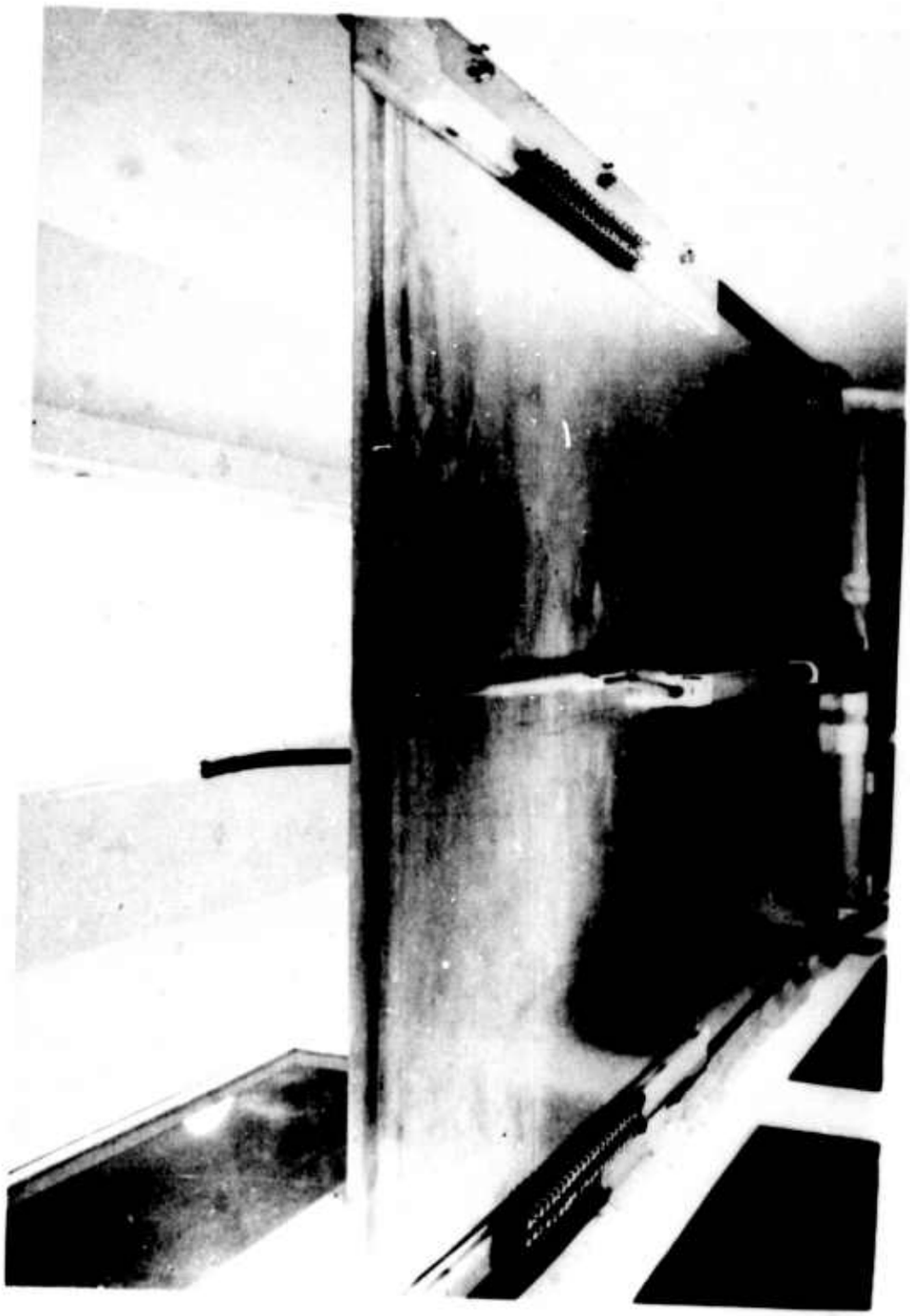

FIGURE 21. UPSTREAM VIEW OF ACTIVE SIDE OF PLATE

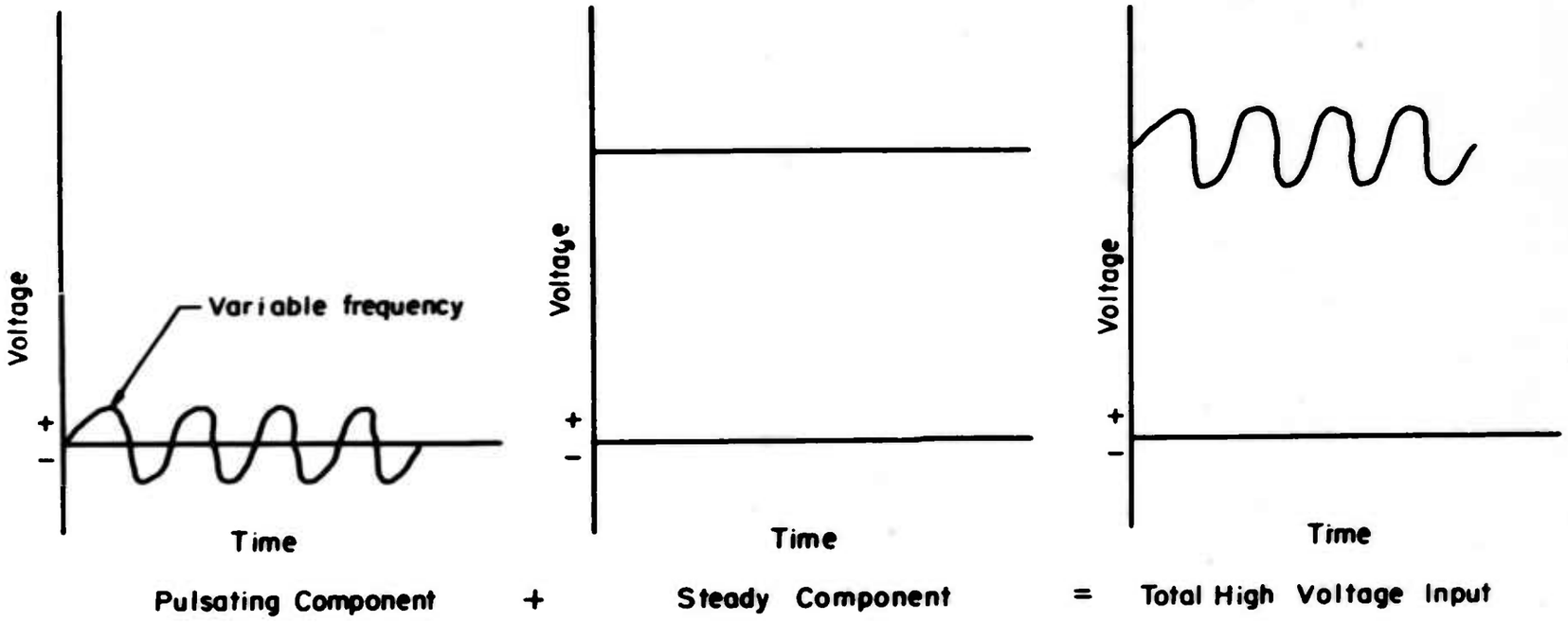

FIGURE 22. PULSATING POTENTIAL IMPOSED ON CORONA WIRES

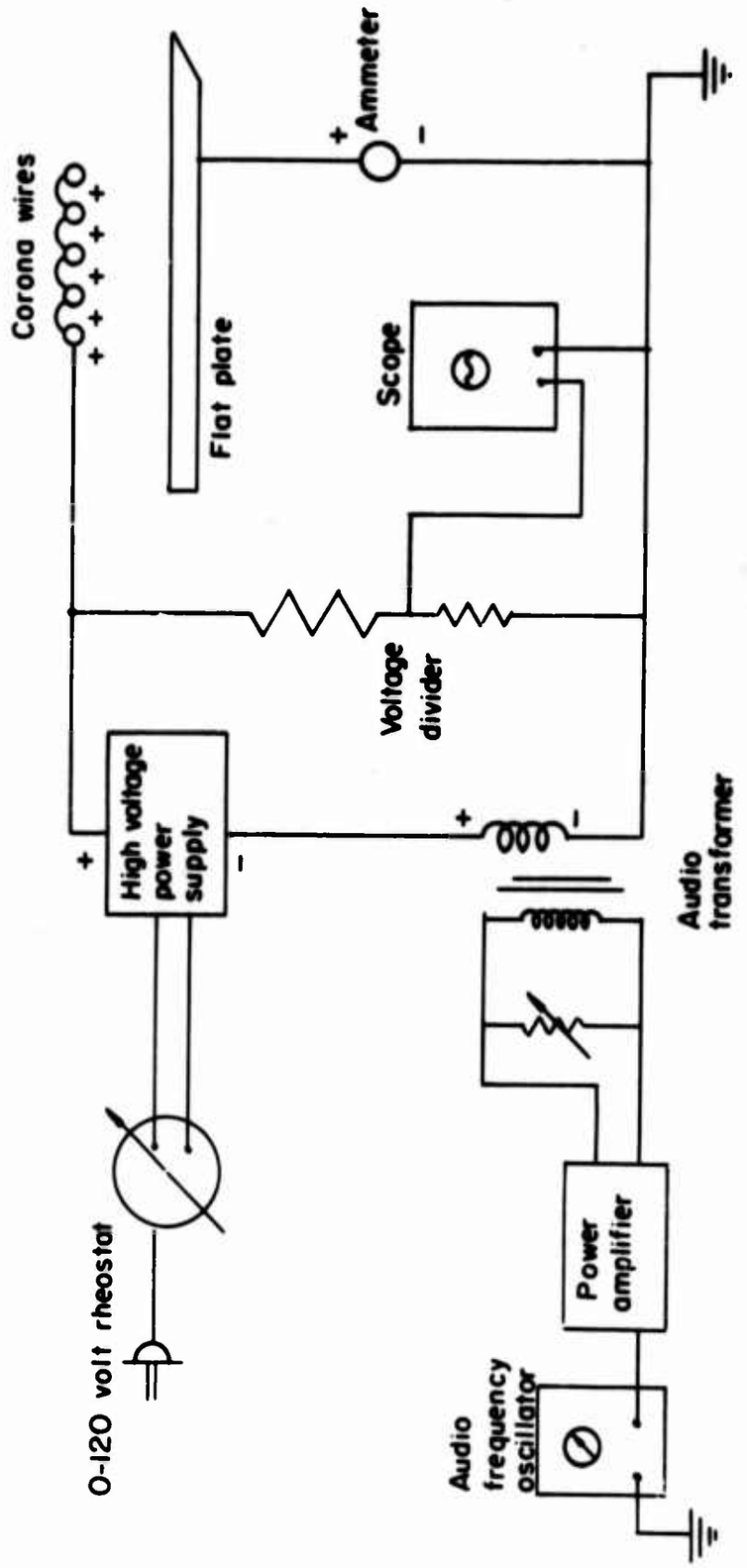

FIGURE 23. CIRCUIT DIAGRAM

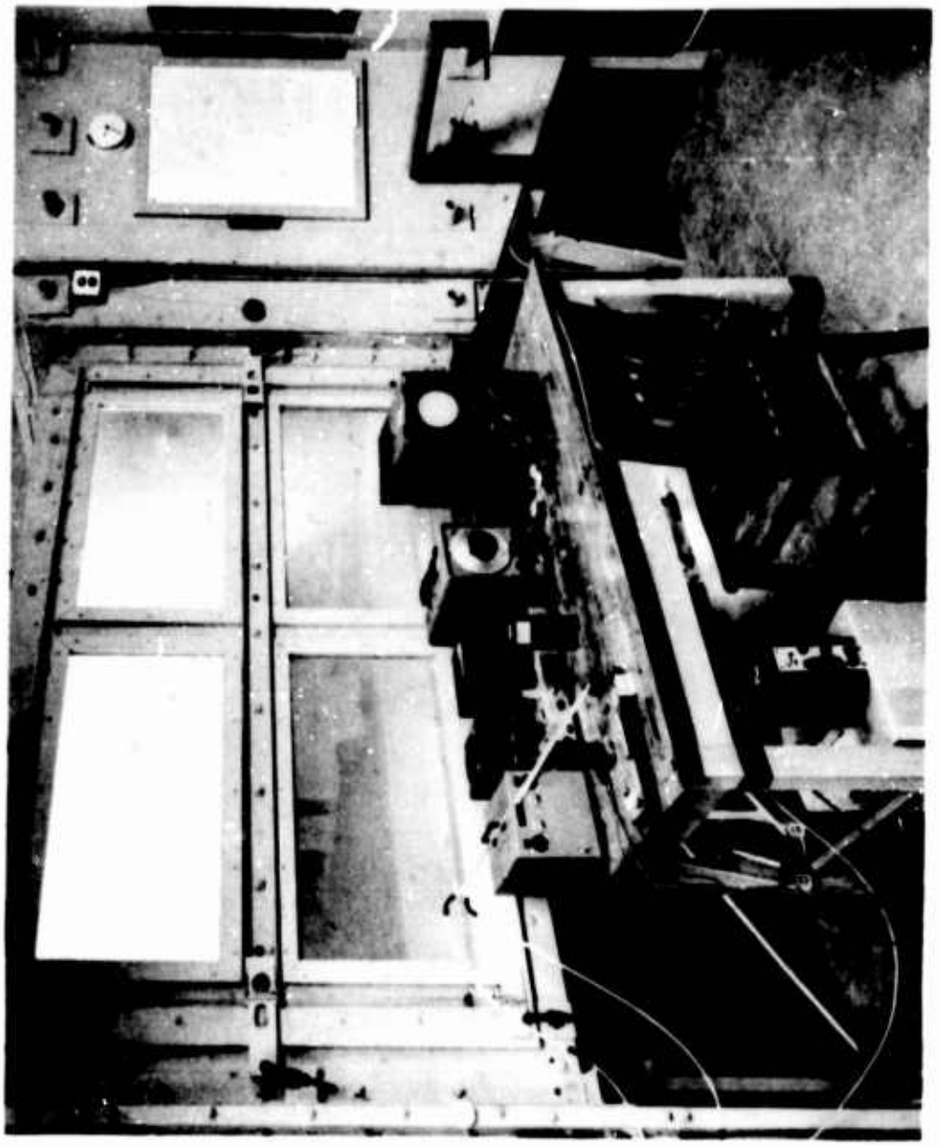

FIGURE 24. ELECTRICAL EQUIPMENT AND TEST SECTION EXTERIOR

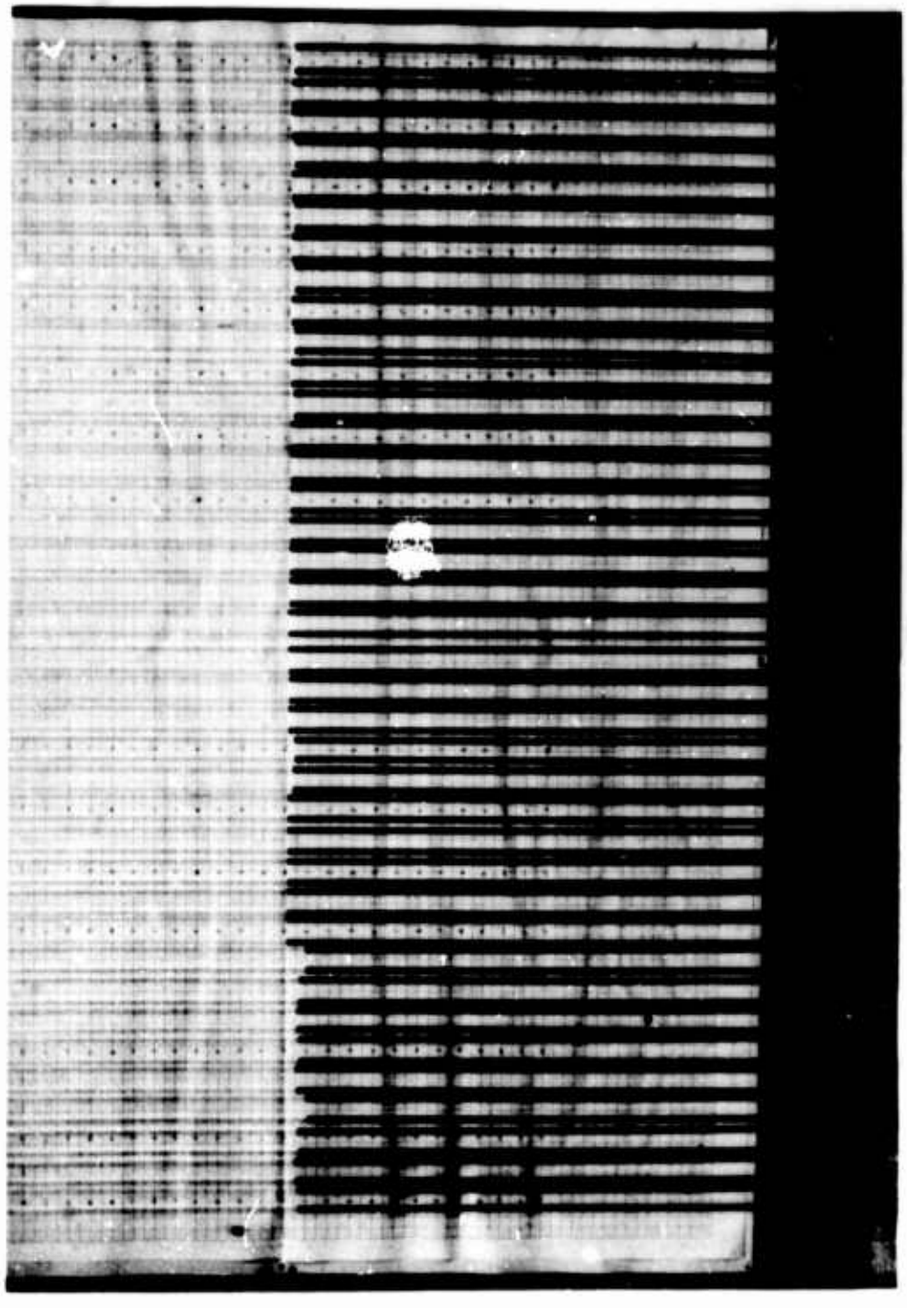

FIGURE 25. MANOMETER BOARD FOR INDICATING STATIC PRESSURE DISTRIBUTION OVER PLATE

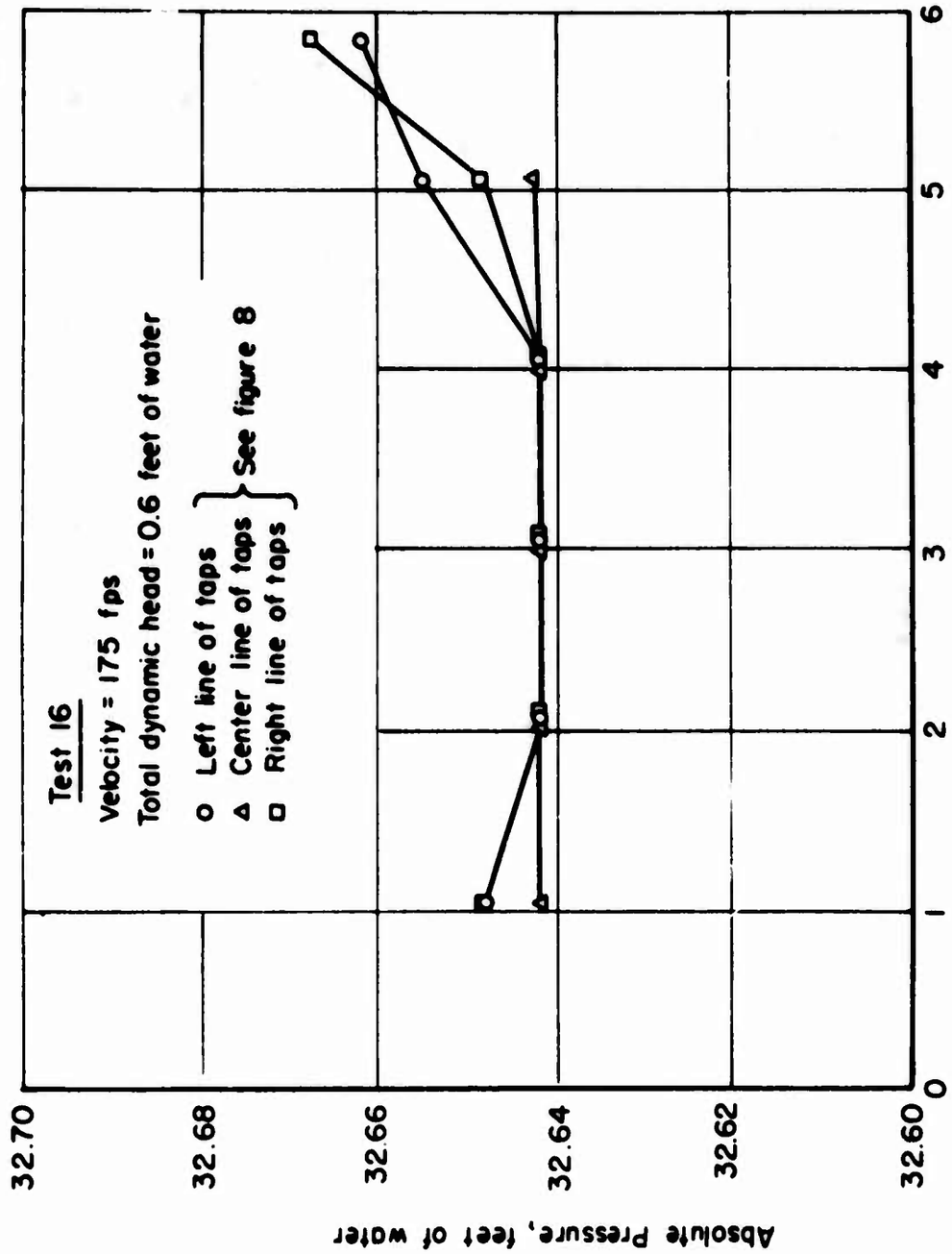

FIGURE 26. TYPICAL STATIC PRESSURE DISTRIBUTION OVER PLATE SURFACE

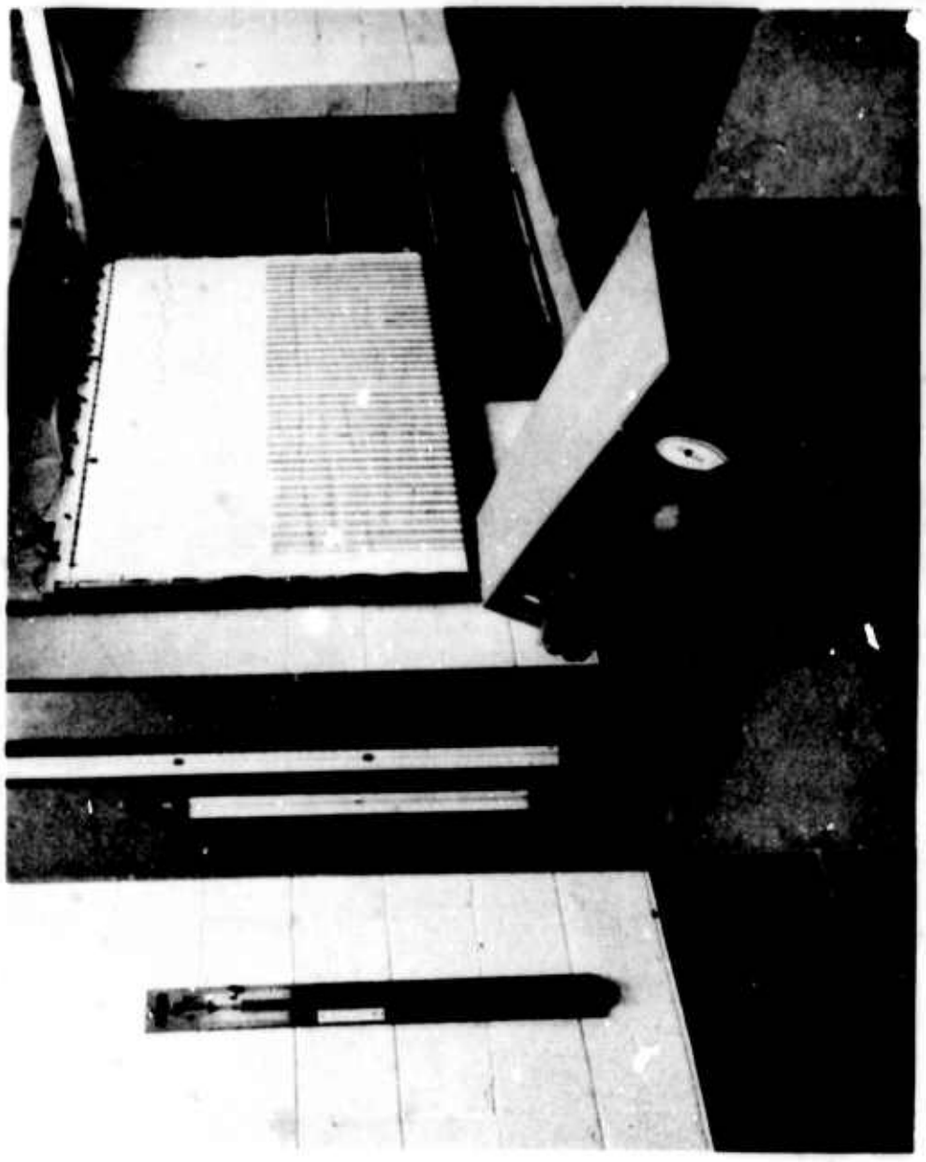

FIGURE 27. TUNNEL CONTROL CONSOLE SHOWING BAROMETER AND FLOW CONTROL MANOMETERS

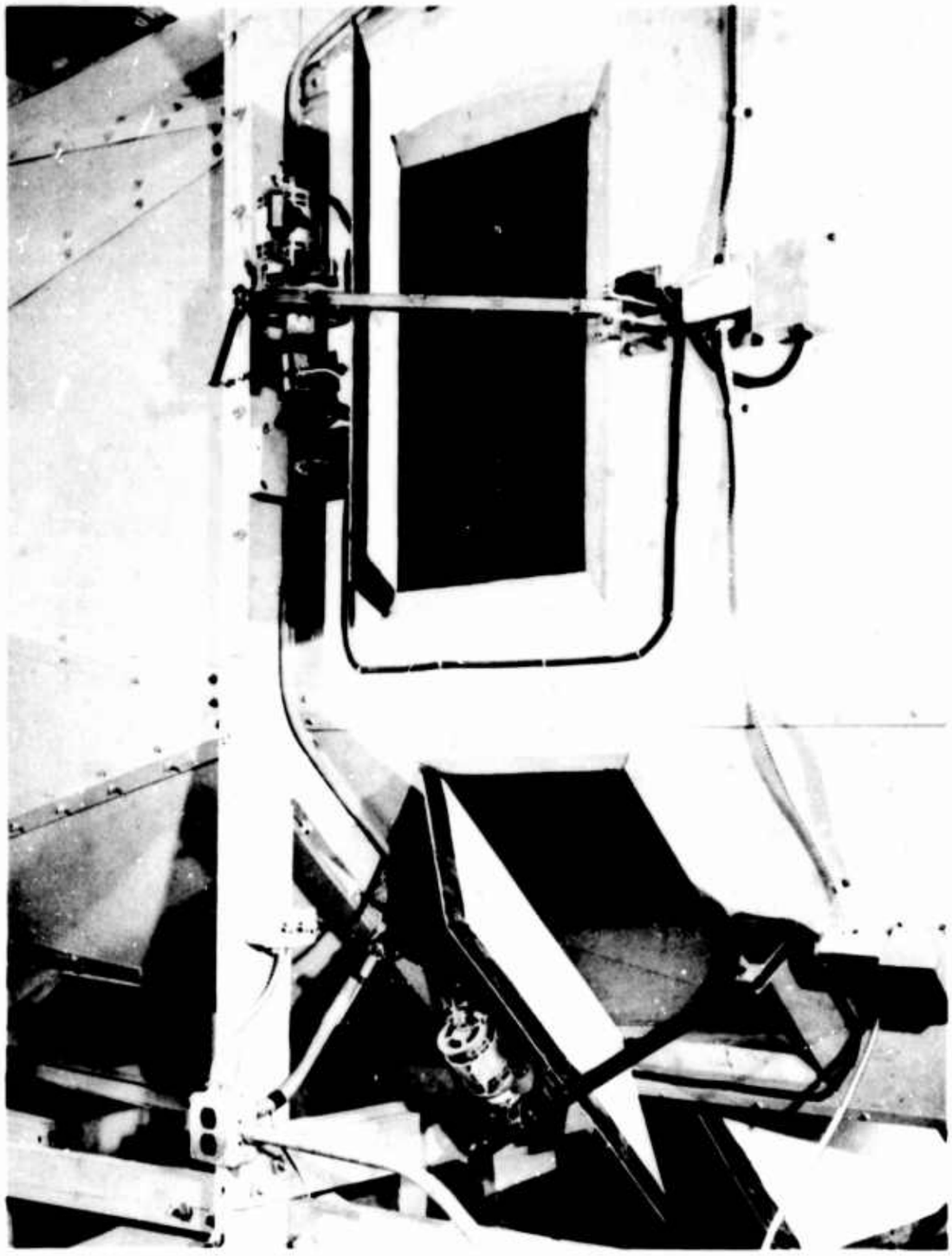

FIGURE 23. WIND TUNNEL FLOW ADJUSTMENT DOORS

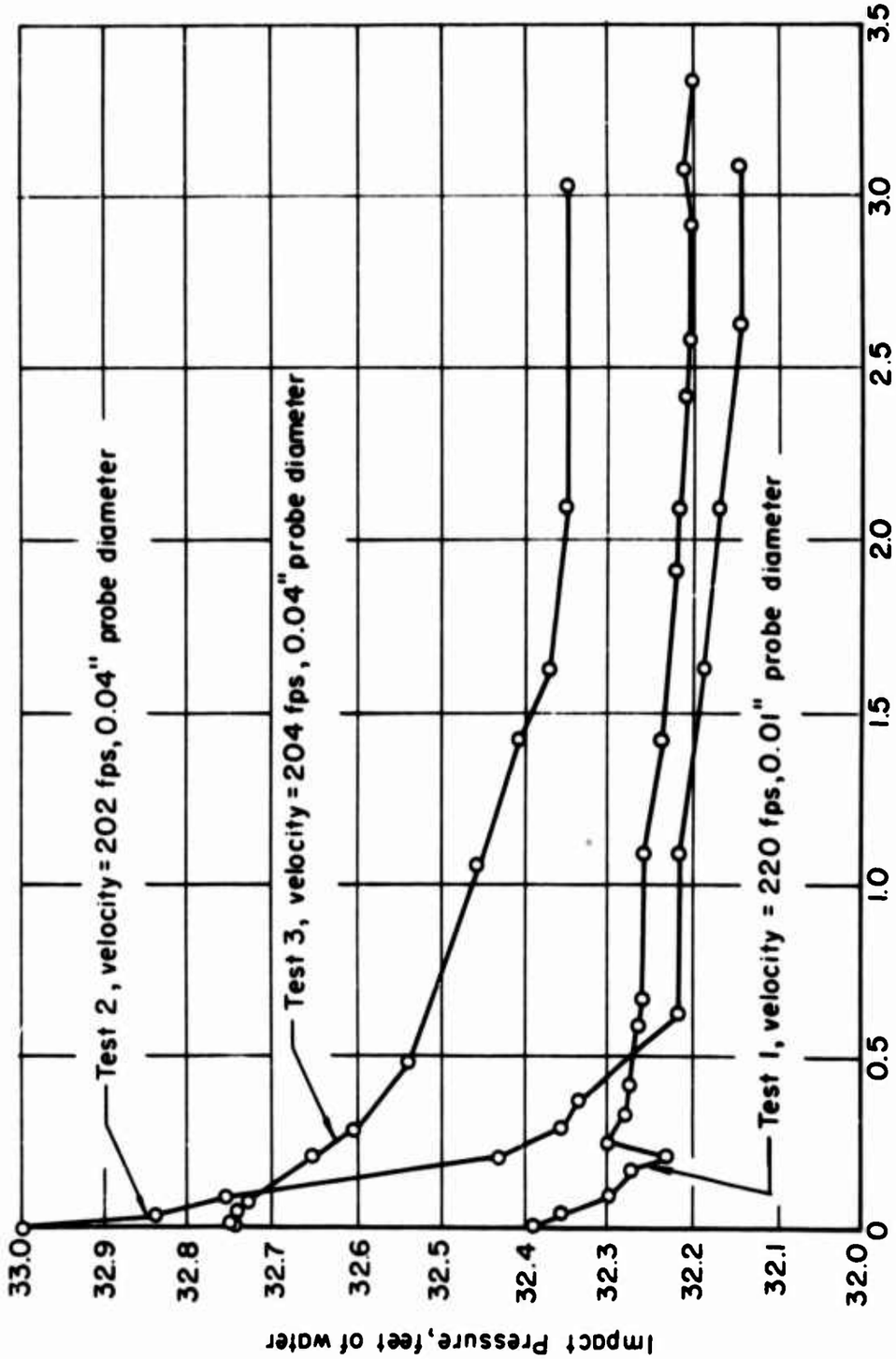

FIGURE 29. NEAR-SURFACE IMPACT PRESSURE WITH ROUNDED LEADING EDGE

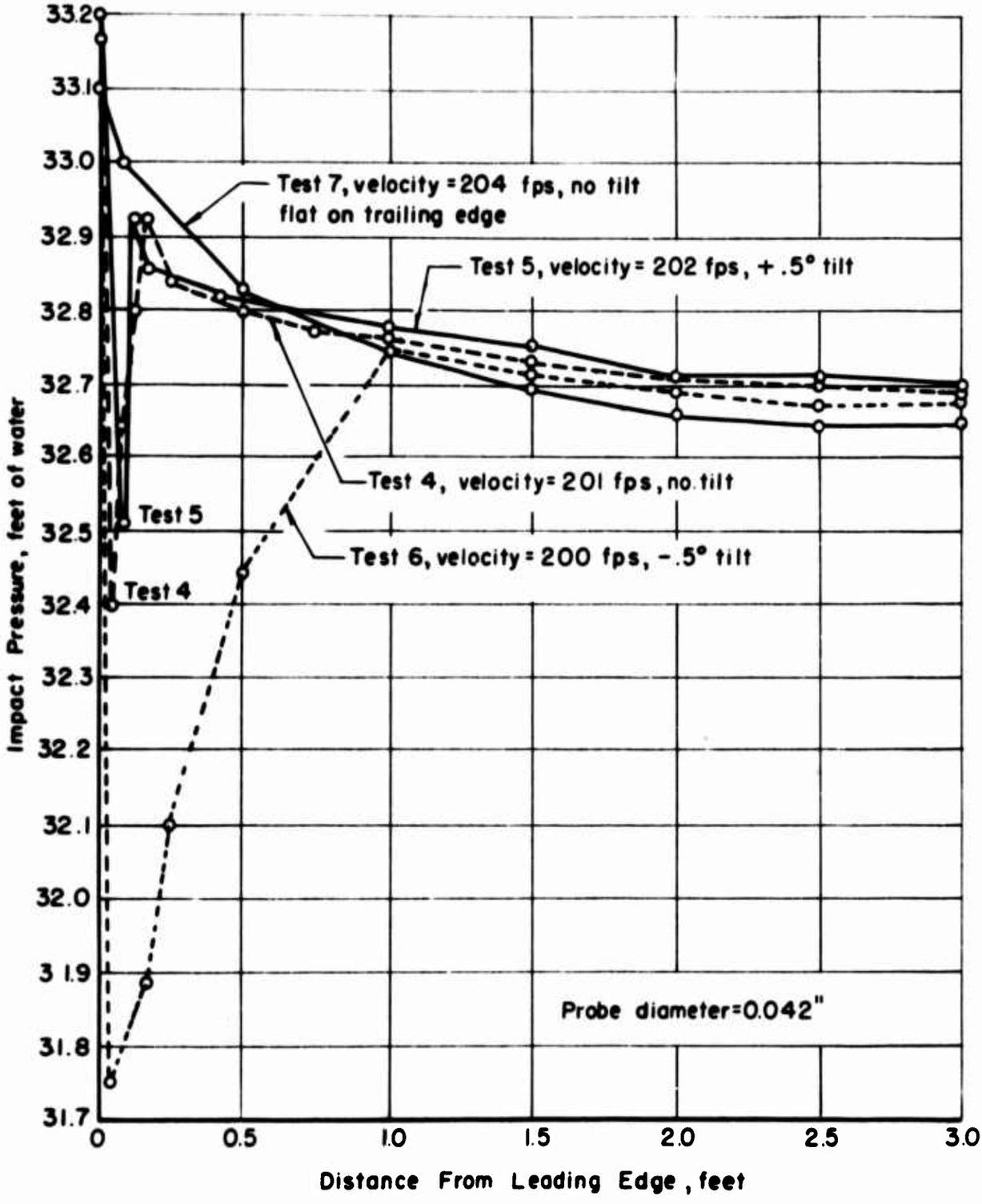

FIGURE 30. NEAR SURFACE IMPACT PRESSURE WITH SHARP LEADING EDGE

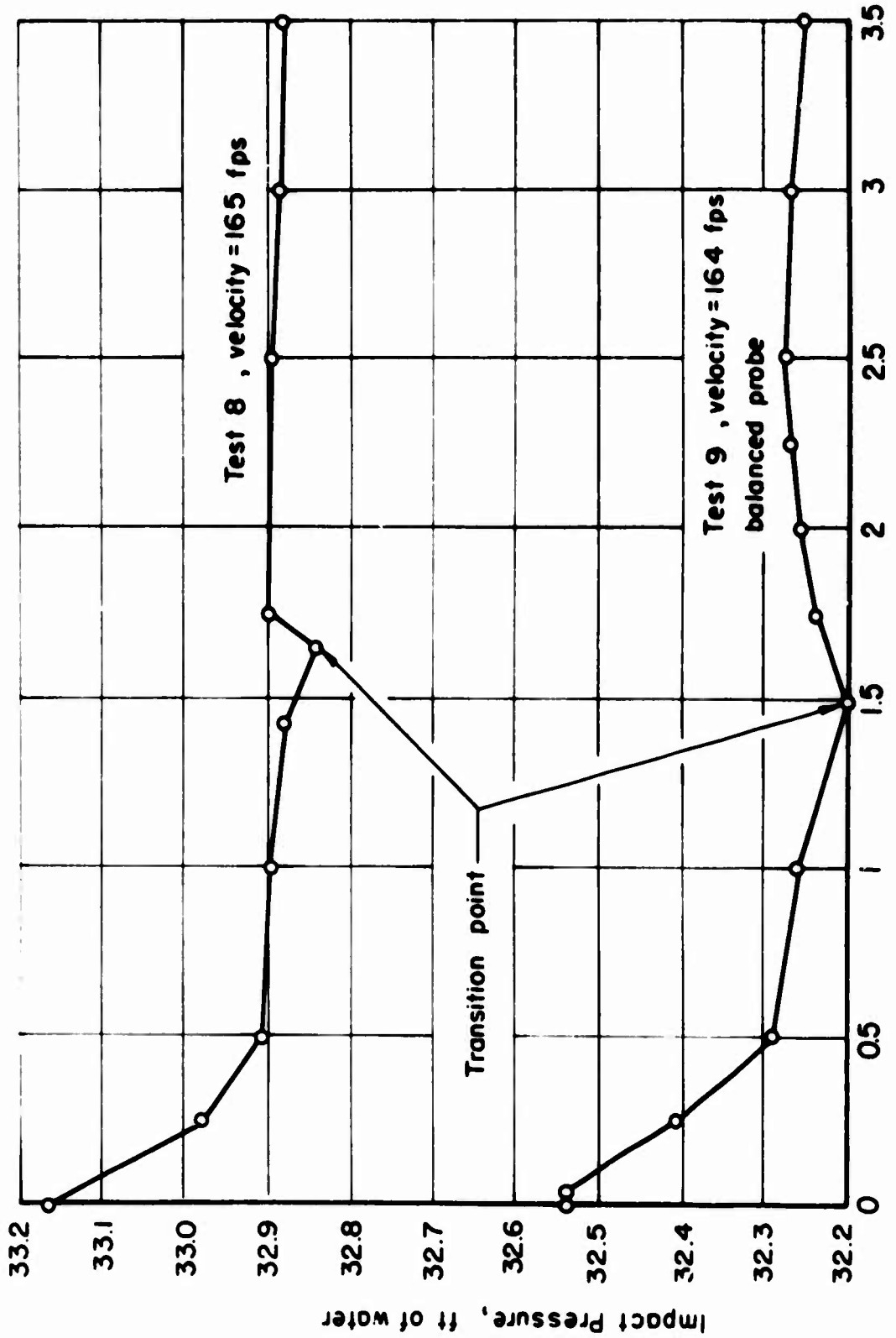

FIGURE 31. TYPICAL IMPACT PRESSURE PROFILES INDICATING BOUNDARY-LAYER TRANSITION

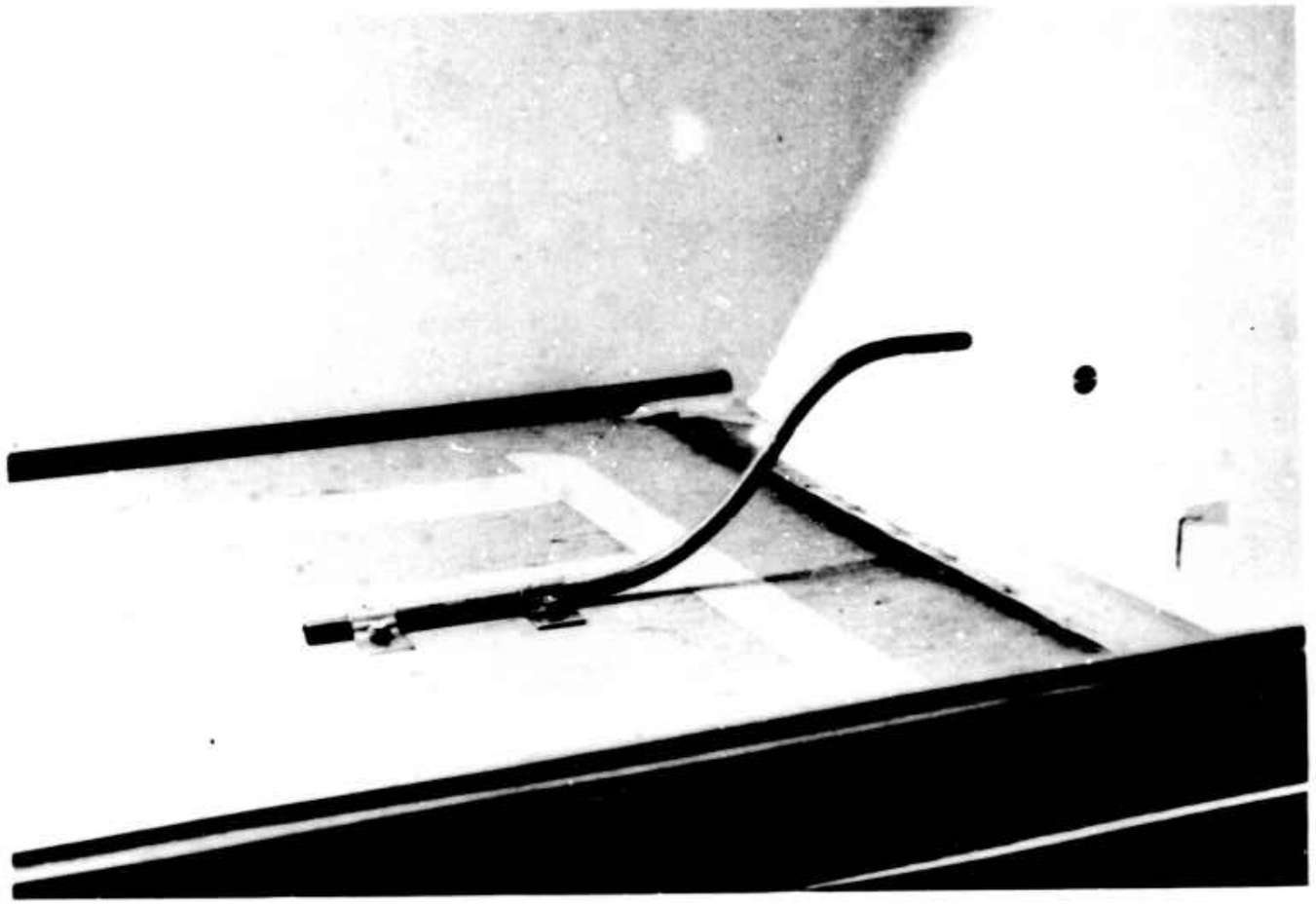

FIGURE 32. TOP SIDE OF PLATE SHOWING STATIONARY IMPACT PRESSURE PROBE

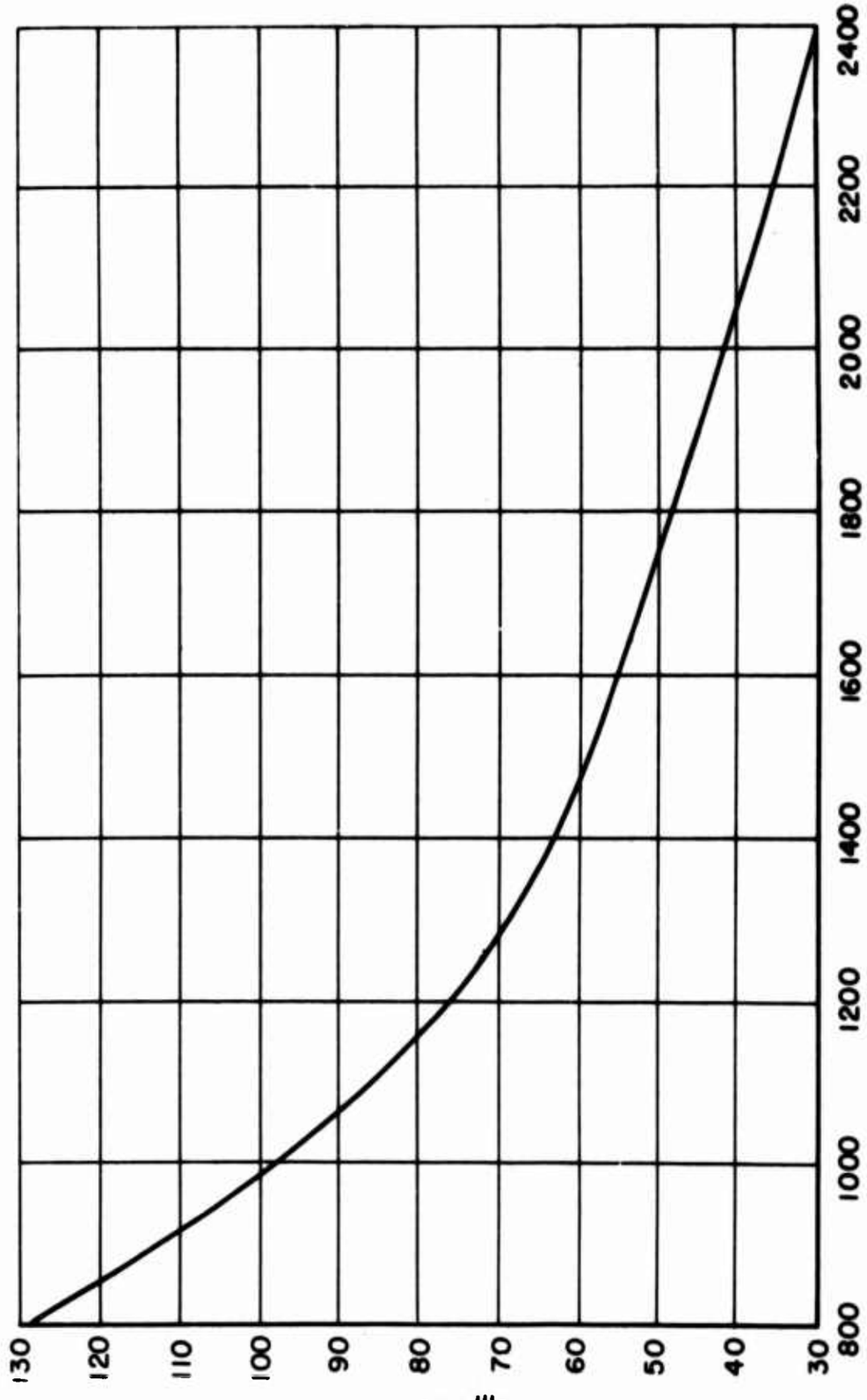

FIGURE 33. FREQUENCY PARAMETER VERSUS REYNOLDS NUMBER FOR $\delta^* = 0.24$.

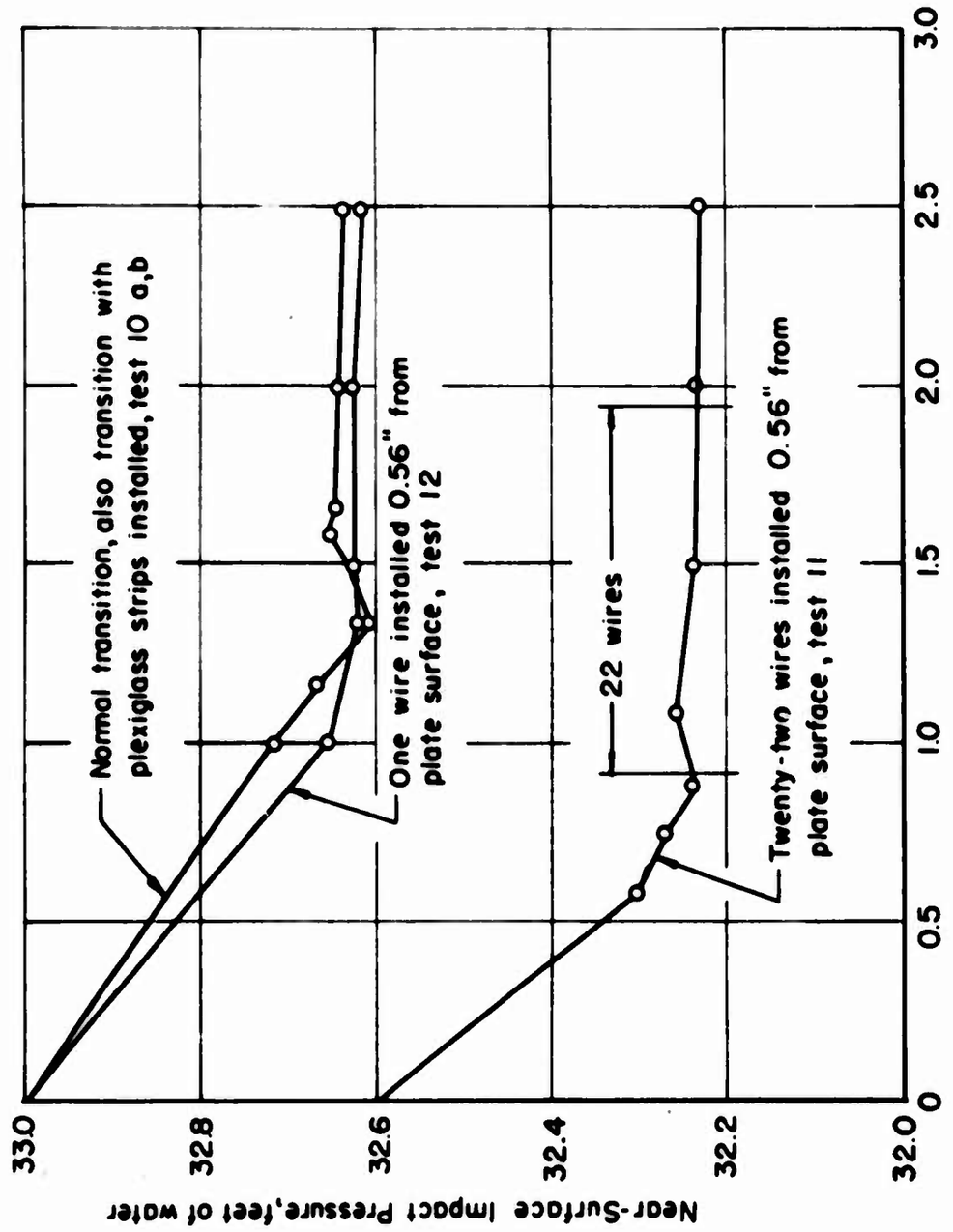

FIGURE 34. CONTROL TESTS, FLOW SPEED 175 FPS

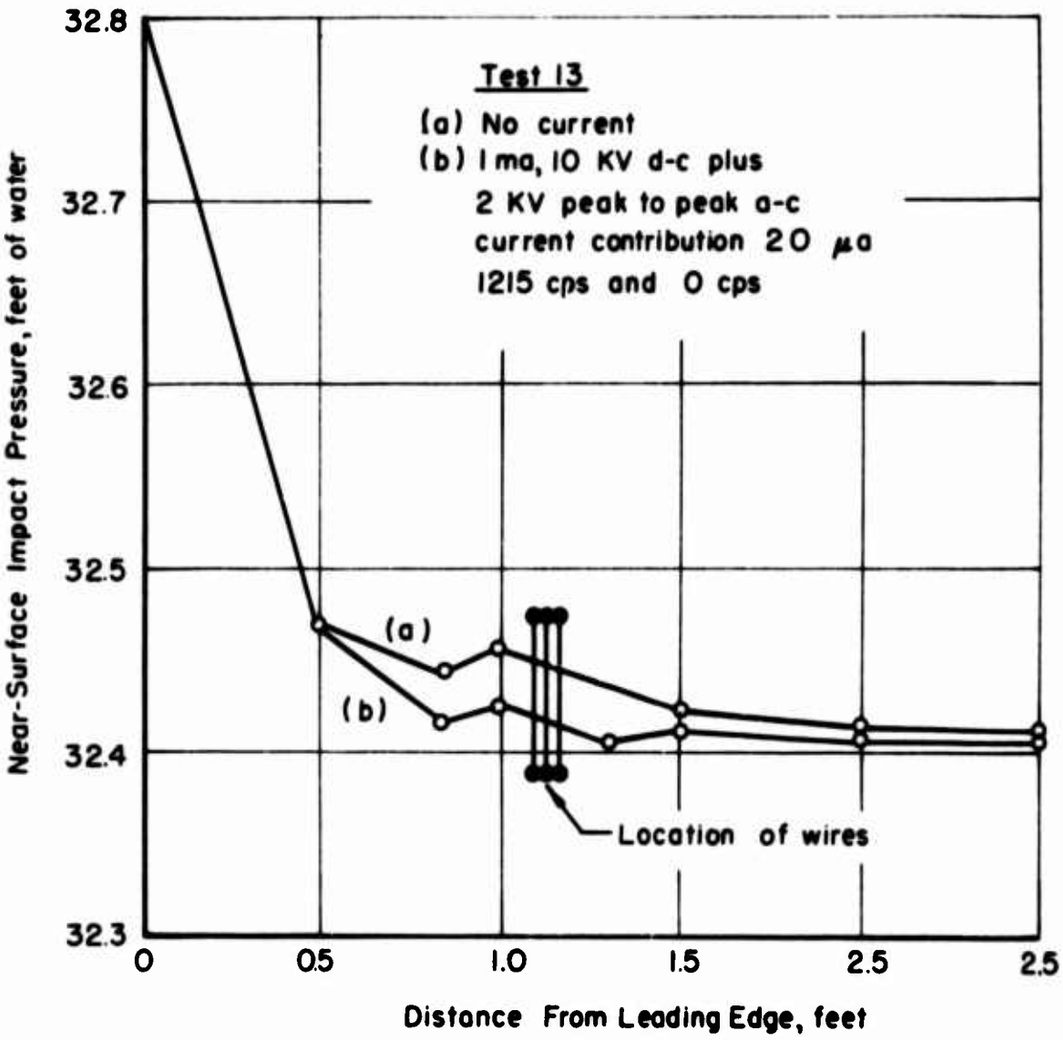

FIGURE 35. CORONA TEST, FLOW SPEED 175 FPS

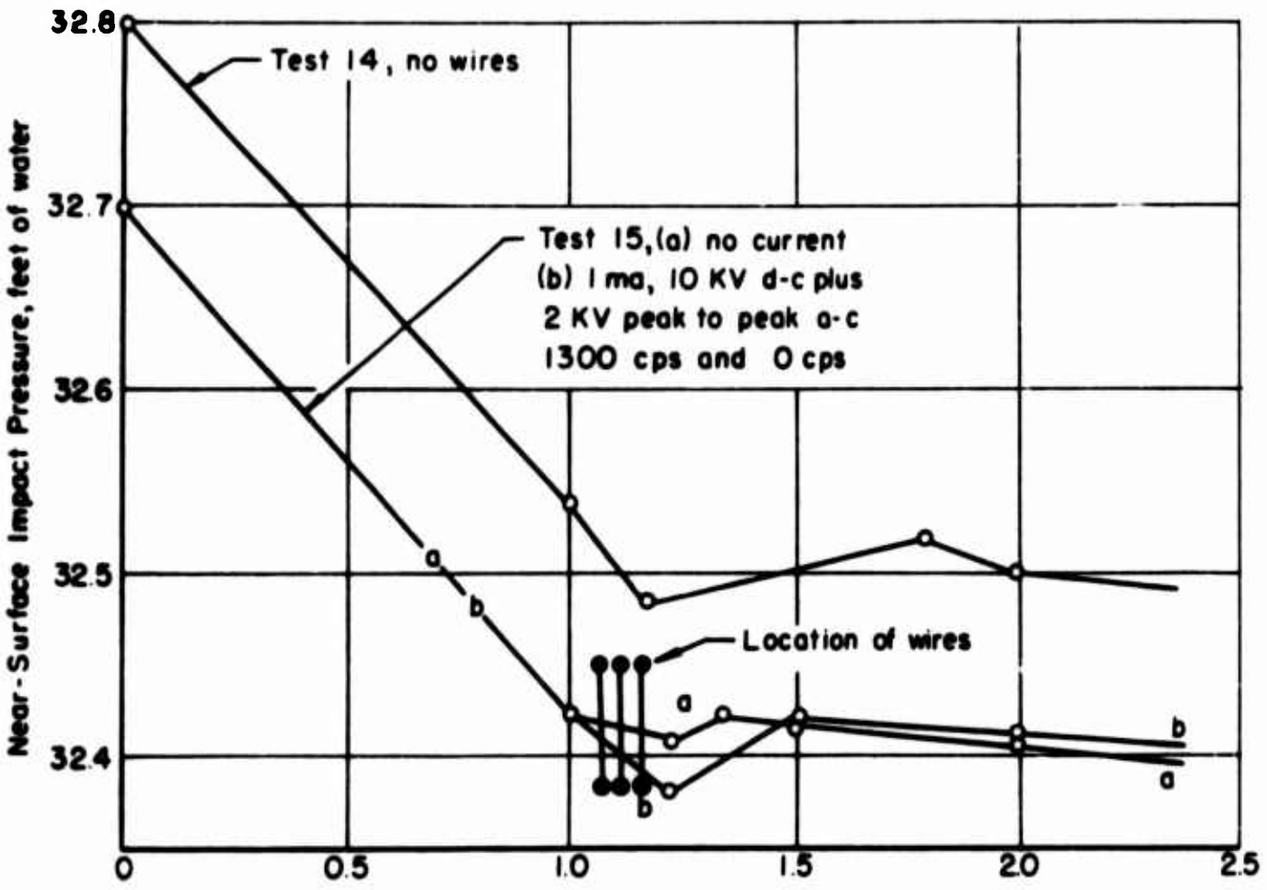

FIGURE 36. CORONA TEST, FLOW SPEED 153 FPS

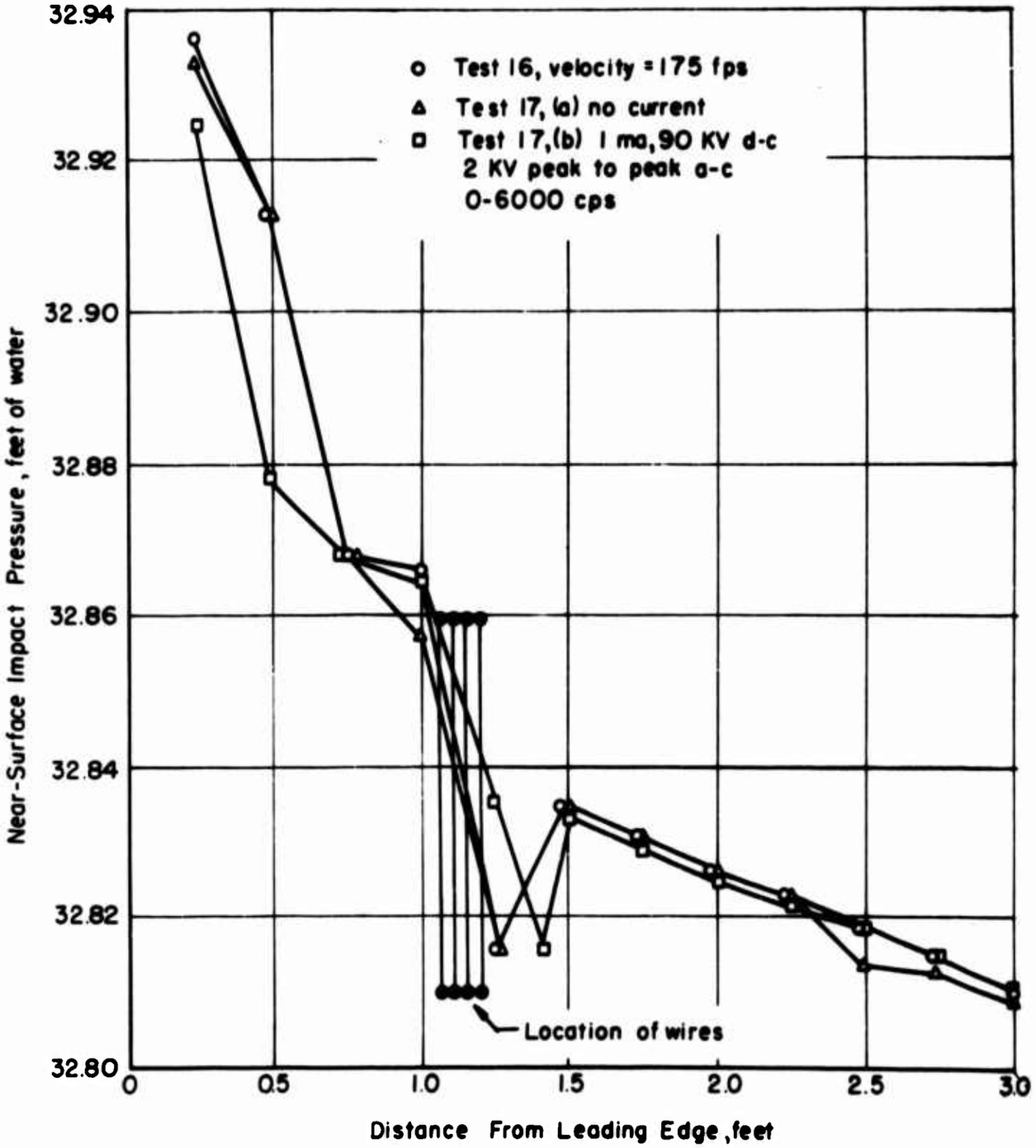

FIGURE 37. SHIFT OF TRANSITION BY CORONA DISCHARGE

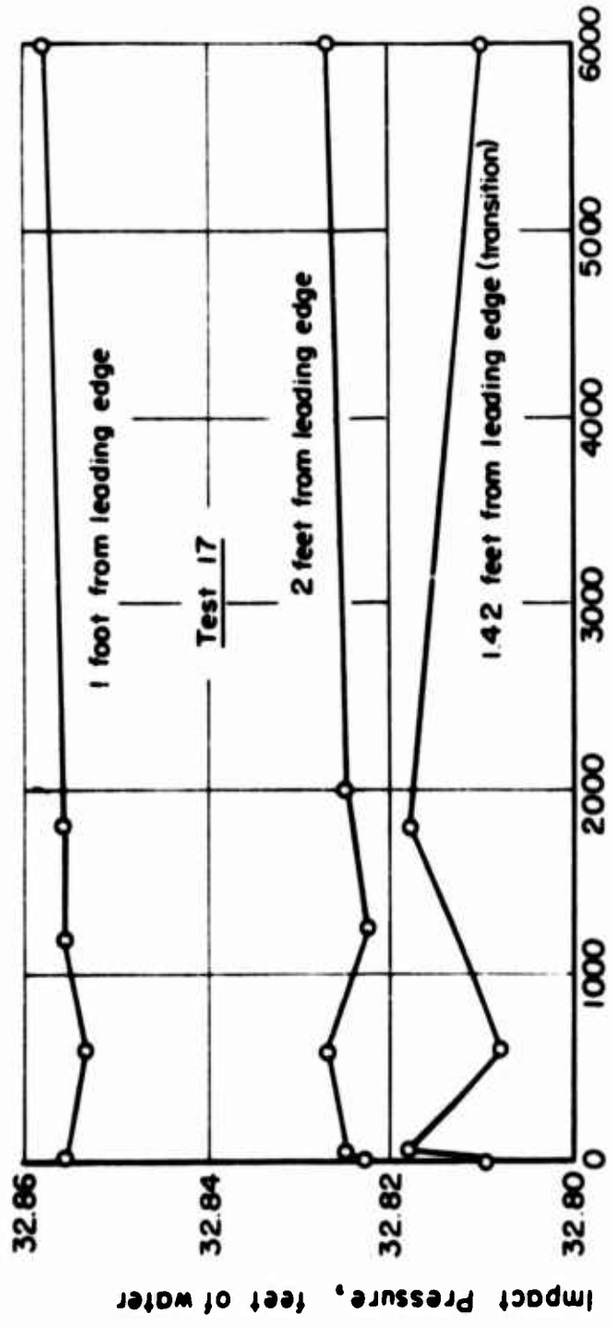

FIGURE 38. IMPACT PRESSURE AS A FUNCTION OF THE FREQUENCY OF THE ELECTRICAL DISTURBANCE

LIST OF REFERENCES

1. Reynolds, O., "An Experimental Investigation of the Circumstances Which Determine Whether the Motion of Water Shall be Direct or Sinuous and of the Law of Resistance in Parallel Channels", Phil. Trans. Roy. Soc. (1883).

2. Bridge, J. F., "A Summary of Parameters Influencing Boundary-Layer Transition", Boeing Airplane Company, Seattle, Washington, Document D2-22052 (1962).

3. Kramer, M. O., "Boundary-Layer Stabilization by Distributed Damping", J. Am. Soc. Naval Engrs., Vol 72, 25-33 (1960).

4. Rogers, O. R., "Aero-Acoustic Aspects of Laminar Flow Control", ASD-TDR-62-718, Vol 1 (1962), WPAFB, Dayton, Ohio.

5. Schubauer, G. B. and Skramstad, H. K., "Laminar-Boundary Layer Oscillations and Transition on a Flat Plate", NACA Report No. 909 (1948).

6. Jackson, F. J. and Heckel, M. A., "Effects of Localized Acoustic Excitation on the Stability of a Laminar-Boundary Layer", ARL Report 62-362 (June, 1962).

7. Schlichting, H., Boundary Layer Theory, McGraw-Hill Book Company, Inc., New York (1955).

8. Lin, C. C., Theory of Hydrodynamic Stability, Cambridge University Press (1955).

9. Gyorgyfalvy, D., "The Possibilities of Drag Reduction by the Use of Flexible Skin", AIAA Paper No. 66-43 (June, 1966).

10. Deimen, J. M. and Clark, J. A., "An Experimental Study of the Influence of Localized, Normal Surface Oscillations on the Laminar Flow Over a Flat Plate", ARL-66-C010, Part VI (1966).

11. Loeb, L. B., Electrical Coronas, University of California Press (1965).

12. Velkoff, H. R., "A New View of Electric Effects on Fluid Dynamics", ASD-TDR-62-718, Volume I (1962), WPAFB, Dayton, Ohio.

13. Eiler, G. P., "An Experimental Investigation of the Influence of Electrostatic Fields on Flow Attachment", The Ohio State University Research Foundation, RF Project 1864, Report No. 4, 1966.

14. Robertson, L. M., "Colorado High Altitude Corona Tests", AIEE Paper No. 57-161, Parts I and II (January, 1957).

15. Werner, J. D. and Geronime, R. L., "Applications of the Corona Discharge for Measurements of Density and Velocity Transients in Air Flow", WADC Technical Report 53-142 (June, 1953).

16. Cobine, J. D., Gaseous Conductors, Dover Publications, Inc., New York (1958).

17. Platt, R. C., "Turbulence Factors of NACA Wind Tunnels as Determined by Sphere Tests", NACA Report 558, 1936.

18. Pope, A., Low Speed Wind Tunnel Testing, John Wiley and Sons, Inc., New York (1966).

19. Kreith, F., Principles of Heat Transfer, International Textbook Company, Scranton (1958).

20. Dean, R. C., Aerodynamic Measurements, Gas Turbine Laboratory, MIT, Cambridge, Massachusetts (1957).

21. Velkoff, H. R., Investigation of the Effects of Electrostatic Fields on Heat Transfer and Boundary Layers, Abstract of Dissertation, The Ohio State University, 1962.

Unclassified

Security Classification

DOCUMENT CONTROL DATA - R&D

(Security classification of title, body of abstract and indexing annotation must be entered when the overall report is classified)

1 ORIGINATING ACTIVITY (Corporate author)	2a REPORT SECURITY CLASSIFICATION
The Ohio State University Research Foundation Columbus, Ohio 43212	Unclassified
	2b GROUP N/A

3 REPORT TITLE

AN EXPERIMENTAL INVESTIGATION OF THE EFFECT OF ELECTRICALLY INDUCED CONTROLLED FREQUENCY PERTURBATIONS ON BOUNDARY LAYER TRANSITION

4 DESCRIPTIVE NOTES (Type of report and inclusive dates)

Technical

5 AUTHOR(S) (Last name, first name, initial)

Ketcham, Jeffrey J.; Velkoff, Henry R.

6 REPORT DATE	7a TOTAL NO OF PAGES	7b NO. OF REFS
June, 1967	101	21

8a CONTRACT OR GRANT NO.	9a ORIGINATOR'S REPORT NUMBER(S)
DA-31-124-ARO-D-246	Technical Report # 5
b PROJECT NO 2001050B700, 1D12140A142	
c	9b OTHER REPORT NO(S) (Any other numbers that may be assigned this report)
d	

10 AVAILABILITY/LIMITATION NOTICES

Distribution of this document is unlimited

11 SUPPLEMENTARY NOTES	12 SPONSORING MILITARY ACTIVITY
	U.S. Army Research Office - Durham Durham, North Carolina

13 ABSTRACT

An experimental investigation was conducted to determine the effects of corona discharge on boundary-layer transition. A flat plate was mounted in Battelle Memorial Institute's low-turbulence wind tunnel. The location of transition was determined using a near-surface impact pressure probe. Boundary-layer excitation was accomplished by suspending a series of corona wires parallel to the plate outside the boundary layer. It was found that, under certain conditions, the transition point could be moved downstream upon application of a steady potential to the wires. Superposition of a pulsating potential did not influence the results over a wide range of pulsation frequency.

DD FORM 1 JAN 64 1473

Unclassified

Security Classification

14 KEY WORDS	LINK A		LINK B		LINK C	
	ROLE	WT	ROLE	WT	ROLE	WT
Corona discharge						
Electro fluid mechanics						
Boundary layer transition						

INSTRUCTIONS

1. ORIGINATING ACTIVITY: Enter the name and address of the contractor, subcontractor, grantee, Department of Defense activity or other organization *(corporate author)* issuing the report.

2a. REPORT SECURITY CLASSIFICATION: Enter the overall security classification of the report. Indicate whether "Restricted Data" is included. Marking is to be in accordance with appropriate security regulations.

2b. GROUP: Automatic downgrading is specified in DoD Directive 5200.10 and Armed Forces Industrial Manual. Enter the group number. Also, when applicable, show that optional markings have been used for Group 3 and Group 4 as authorized.

3. REPORT TITLE: Enter the complete report title in all capital letters. Titles in all cases should be unclassified. If a meaningful title cannot be selected without classification, show title classification in all capitals in parenthesis immediately following the title.

4. DESCRIPTIVE NOTES: If appropriate, enter the type of report, e.g., interim, progress, summary, annual, or final. Give the inclusive dates when a specific reporting period is covered.

5. AUTHOR(S): Enter the name(s) of author(s) as shown on or in the report. Enter last name, first name, middle initial. If military, show rank and branch of service. The name of the principal author is an absolute minimum requirement.

6. REPORT DATE: Enter the date of the report as day, month, year, or month, year. If more than one date appears on the report, use date of publication.

7a. TOTAL NUMBER OF PAGES: The total page count should follow normal pagination procedures, i.e., enter the number of pages containing information.

7b. NUMBER OF REFERENCES: Enter the total number of references cited in the report.

8a. CONTRACT OR GRANT NUMBER: If appropriate, enter the applicable number of the contract or grant under which the report was written.

8b, 8c, & 8d. PROJECT NUMBER: Enter the appropriate military department identification, such as project number, subproject number, system numbers, task number, etc.

9a. ORIGINATOR'S REPORT NUMBER(S): Enter the official report number by which the document will be identified and controlled by the originating activity. This number must be unique to this report.

9b. OTHER REPORT NUMBER(S): If the report has been assigned any other report numbers *(either by the originator or by the sponsor)*, also enter this number(s).

10. AVAILABILITY/LIMITATION NOTICES: Enter any limitations on further dissemination of the report, other than those imposed by security classification, using standard statements such as:

(1) "Qualified requesters may obtain copies of this report from DDC."

(2) "Foreign announcement and dissemination of this report by DDC is not authorized."

(3) "U. S. Government agencies may obtain copies of this report directly from DDC. Other qualified DDC users shall request through _____."

(4) "U. S. military agencies may obtain copies of this report directly from DDC. Other qualified users shall request through _____."

(5) "All distribution of this report is controlled. Qualified DDC users shall request through _____."

If the report has been furnished to the Office of Technical Services, Department of Commerce, for sale to the public, indicate this fact and enter the price, if known.

11. SUPPLEMENTARY NOTES: Use for additional explanatory notes.

12. SPONSORING MILITARY ACTIVITY: Enter the name of the departmental project office or laboratory sponsoring *(paying for)* the research and development. Include address.

13. ABSTRACT: Enter an abstract giving a brief and factual summary of the document indicative of the report, even though it may also appear elsewhere in the body of the technical report. If additional space is required, a continuation sheet shall be attached.

It is highly desirable that the abstract of classified reports be unclassified. Each paragraph of the abstract shall end with an indication of the military security classification of the information in the paragraph, represented as *(TS), (S), (C), or (U)*.

There is no limitation on the length of the abstract. However, the suggested length is from 150 to 225 words.

14. KEY WORDS: Key words are technically meaningful terms or short phrases that characterize a report and may be used as index entries for cataloging the report. Key words must be selected so that no security classification is required. Identifiers, such as equipment model designation, trade name, military project code name, geographic location, may be used as key words but will be followed by an indication of technical context. The assignment of links, rules, and weights is optional.